The study of electromagnetic processes in the experiments of Tesla

B. Sacco[1], A.K. Tomilin [2],

[1] RAI, Center for Research and Technological Innovation
(Turin, Italy), *b.sacco@rai.it*
[2]National Research Tomsk Polytechnic University
(Tomsk, Russian Federation)*, aktomilin@gmail.com*

The Tesla wireless transmission of energy original experiment, proposed again in a downsized scale by K. Meyl, has been replicated in order to test the hypothesis of the existence of electroscalar (longitudinal) waves. Additional experiments have been performed, in which we have investigated the features of the electromagnetic processes between the two spherical antennas. In particular, the origin of coils resonances has been measured and analyzed. Resonant frequencies calculated on the basis of the generalized electrodynamic theory, are in good agreement with the experimental values found.

Keywords: Tesla transformer, K. Meyl experiments, electroscalar waves, generalized electrodynamics, coil resonant frequency.

1. Introduction

In the early twentieth century, Tesla conducted experiments in which he demonstrated unusual properties of electromagnetic waves. Results of experiments have been published in the newspapers, and many devices were patented (e.g. [1]). However, such work has not received suitable theoretical explanation, and so far no practical application of the results have been developed.

One hundred years later, Professor K. Meyl [2] aimed to reproduce the same experiments using a miniature, laboratory version of the Tesla setup, arguing that it can help to detect unusual phenomena that are explained by the presence of electroscalar (longitudinal) waves, namely:

- the reaction on the transmitter of the presence of the receiver;
- the transmission of scalar waves with a speed of 1,5 times the speed of light;
- the inefficiency of a Faraday cage in shielding scalar waves, and
- the possibility of wireless transmission of electrical energy.

Nearly ten years have passed since the publication of the results of K. Meyl experiments. However, despite this, they still have not received a clear theoretical explanation. Some authors, for example [3], believe that the observed phenomena can be explained on the basis of the properties of ordinary transverse electromagnetic waves. It has been suggested that the set-up of K. Meyl does not play all the experimental conditions of Tesla.

Are there really unexplored components of the electromagnetic wave? Under what conditions do they occur? Which are their properties? These are important questions that remain open. From the answers depend our assessment of the current state of electrodynamics and science in general. In this situation it

is needed a balanced and pragmatic approach allowing to take into account all the correct facts and give them the correct interpretation.

The relevance of setting and study the issues raised above is now obvious. There are a lot of experimental facts and theoretical considerations that require interpretation. The so-called electroscalar waves have been observed in the experiments carried on by C. Monstein and J. P. Wesley [4], and by G.V. Nikolaev [5]. Theoretical substantiation of the physical meaningfulness of the electroscalar waves is contained in N.P. Hvorostenko [6], A.K. Tomilin [7-9], Koen J. van Vlaenderen [10], D.A. Woodside [11]. The problem of experimental detection electroscalar waves is also dealt with by G. Bettini [17]. Interesting results are contained in the Elmore G. paper [18].

This work includes experimental and theoretical parts. The basic K. Meyl experiments have been reproduced, and supplemented with new experiments to detect and describe the phenomena that cannot be explained on the basis of modern electromagnetic field theory. The included theoretical analysis is based on a generalized theory aimed to complete the modern electrodynamics for encompassing all known (including the little-studied) experimental facts and natural phenomena.

2. The K. Meyl experiments summary

The system originally proposed by Tesla [1] (Fig. 1) consisted of a transmitter including a resonant transformer with a strong elevation of potential: the *high inductance spiral secondary coil*, loaded by a *low capacitance "elevated" metal sphere*, was coupled to a *low inductance spiral primary coil*[1]. The transmitter primary was driven by a high frequency, high voltage supply. The receiver was identical and symmetrical. The load was e.g. a set of lamps connected in parallel at the receiver output. As affirmed by Tesla himself, the ground connection in this structure plays an important role.

With this structure Tesla did actually demonstrate something that today would be unthinkable to be done with Hertz radio waves: in Colorado Springs he built two towers, one 10 kW transmitter and a receiver located at a distance of 25 miles, and he demonstrated that it could be receive substantially 100% of the transmitted power, in facts, he could power 200 fluorescent lamps of 50 watts each. The experiment was published in the contemporary newspapers.

K. Meyl [2] experiment is inspired by Nikola Tesla patent mentioned above. In fact, the structure used is a miniature version (but not on scale) of the receiver and transmitter towers of the original installation of Tesla. Here, however, the size of the "towers" is about thirty centimeters. Each tower has a flat Tesla coil in its base plate, consisting of a two turns spiral primary coil and a many turns spiral secondary coil, made on a single printed circuit board. A

---

[1] In some implementations by Tesla himself, the primary was brought to resonance adding high-capacity capacitors in parallel.

sphere with metal surface is placed on top, connected by a wire to the inner end of the secondary.
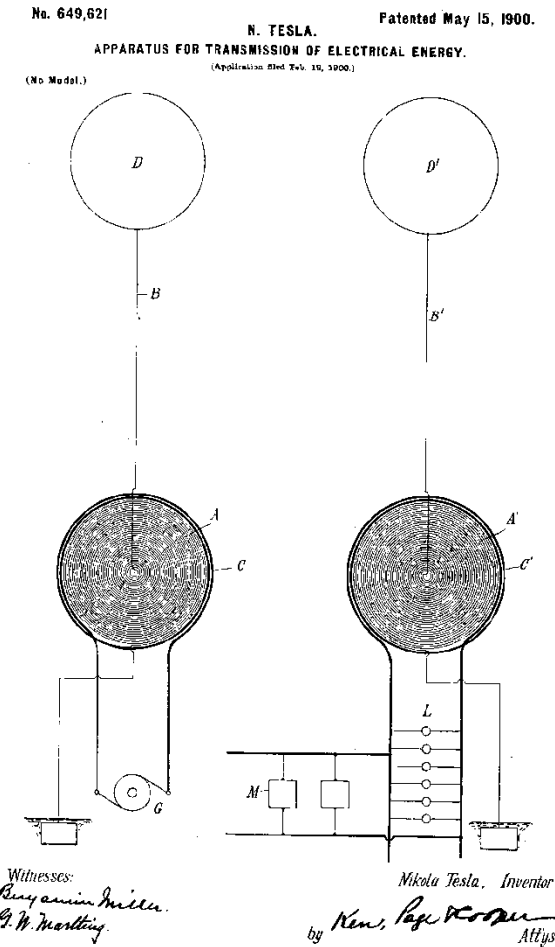
Fig. 1

In order to make precise measurements of frequency, Meyl adopted a small synthesized frequency generator with digital readout. Due to the relatively small size of the equipment, the frequency range of the resonance that results is in the order of a few *MHz*, while Tesla was working at frequencies much lower. In addition, these small-scale demonstration devices are fed with signals voltage of about 2 *V*, while Tesla, in his great power wireless transmission installation, used about 60 *kV* supply (the antenna potential being much higher).

In Fig. 2 is outlined the structure adopted by Meyl. The RF generator is connected in parallel to the primary of the Tesla Coil (TC) transmitter, two LEDs in anti-parallel are connected across TC input too. The TC secondary is isolated from the primary. The inner end, as already mentioned, is connected to the metal ball; the outer one is connected to the "earth", which in this experiment is emulated, in a "degenerate" way, with a single copper wire that reaches the receiver.
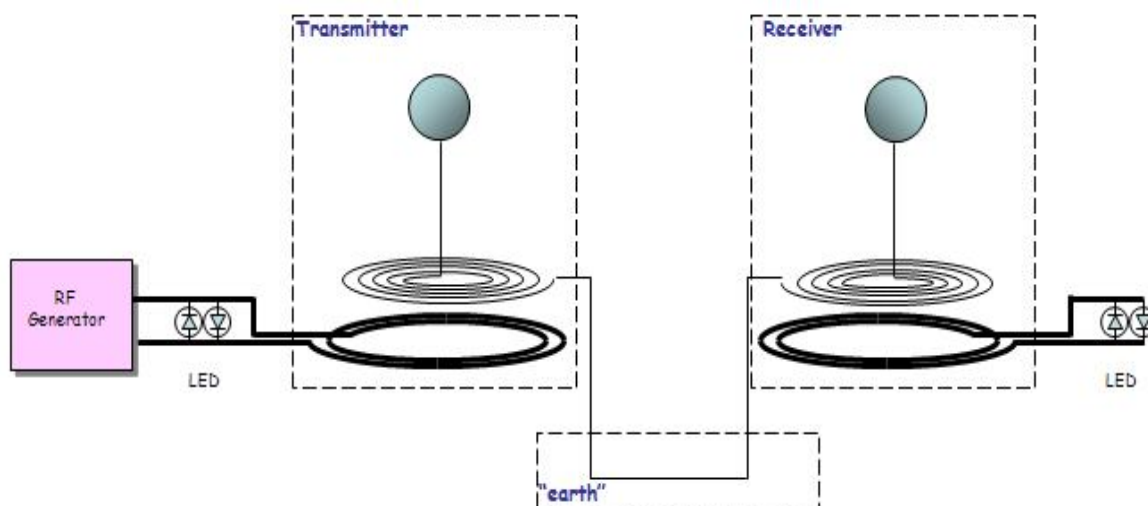
Fig. 2

The transmitter and receiver are completely symmetric. As a "load" two LEDs are connected in anti-parallel, symmetric and similar to those present at the transmitter. Photo set K. Meyl shown in Fig. 3.
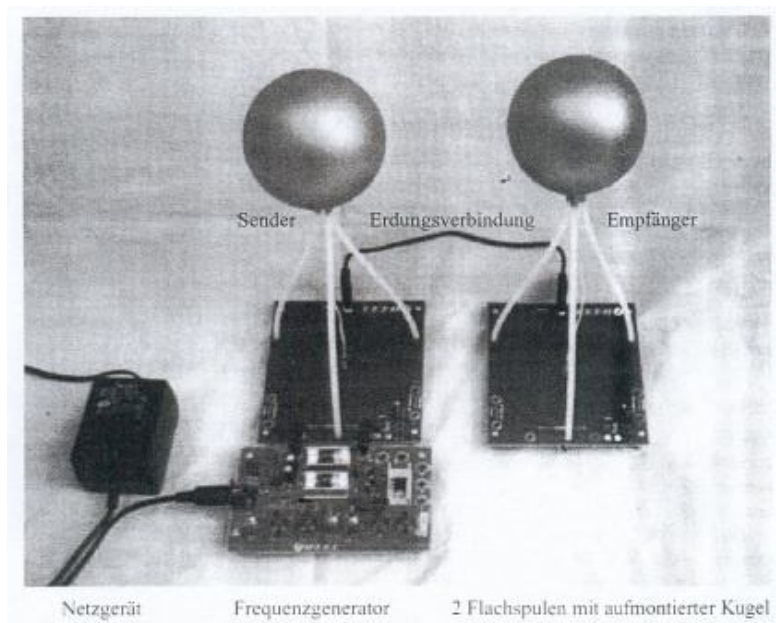

Fig. 3

In his experiment, K. Meyl has adopted the following procedure:
• First step: The output level of the generator set to approximately $2V$. The generator frequency is adjusted, until the resonant frequency are detected by the brightness of the LEDs on the receiver. The [main, higher] resonance is found at a frequency $f_{02} = 7MHz$. At the resonance, the transmitter LEDs turn off.
• Second step: Then the receiver earth wire is disconnected. In this case the receiver LEDs are extinguished and the transmitter will light up brightly. That

is, the transmitter "feels" if the receiver receives the signal. K. Meyl called it *"a reaction to the receiver back to the transmitter."*

• Third step: tuning down the frequency, another resonance is found at $f_{01} = 4,7 MHz$; here the receiver LEDs are less shining, and the signal is easily screened. The reverse reaction of the transmitter to the receiver is absent.

Professor K. Meyl interprets the phenomena described above as follows.

In the first step of the procedure, adjusting the frequency generator to the appropriate frequency, it results:

> *a)* receiver LED lights up. Meyl interpretation: "*In this condition the energy transfer takes place*";
>
> *b)* simultaneous fading down of the transmitter's LED. Meyl interpretation: *"Back-reaction of the receiver on the transmitter"*.

In the second step of the procedure, the transmitter LED lights again, when the operator disconnects the receiver. Meyl interpretation: *"This is a proof of the back-reaction of receiver on the transmitter"*.

In the third step, for the resonance at lower frequency, $f_{01} = 4,7 MHz$, it is highlighted that occurs:

> *a)* lower intensity of the LED,
>
> *b)* signal can be easily shielded,
>
> *c)* lack of marked back-reaction on the transmitter.

Meyl interpretation for points *a,b,c* above: *"This is conventional, Hertzian waves. This is a proof that scalar waves speed (for resonance at 7MHz) is higher than the one of Hertzian waves (resonance at 4.7MHz). In particular, scalar waves speed results 7/4,7=1,5 times the speed of light[2] "*.

3. Replication of the K. Meyl experiments and discussion

3.1 Basic replication

The K. Meyl experiment has been replicated in the laboratory of the Rai Research and Technological Innovation Cent (*Italy*). From the cited paper not the all parameters of the TC are disclosed, but, under the likely hypothesis that from the geometrical dimensions will depend only the resonance frequencies, not the overall behavior of the system, it was decided to proceed building two pairs of coils with size roughly similar to the Meyl's ones, thus accepting some uncertainty margin.

We used a standard sinusoidal signal generator HP33120A. As indicators, the LEDs were first used. Initially, the entire apparatus was placed on the bench, the distance between transmitter and receiver being quite limited (approximately 0.5 *m*).

---

[2]No explanations is given in the paper.

Transmitter	
Primary	
Winding type	Counter-clockwise spiral
Number of turns	2 turns
Wire type	Copper ribbon, 8*mm* x 0.5*mm*
Inner diameter	150*mm*
Outer diameter	163*mm*
Secondary	
Winding type	Counter-clockwise spiral
Number of turns	31 turns
Wire type	coax cable, 1.3*mm* diameter (1.7*mm* including outer insulation; outer + inner conductors used together as single conductor)
Inner diameter	10*mm*
Outer diameter	117*mm*
Antenna	
Pole	Bakelite tube, l= 195*mm* with internal wire.
Sphere	63*mm* polystyrene sphere coated with aluminium foil
Receiver	
Primary	
Winding type	clockwise spiral
Number of turns	Same as Tx
Wire type	Same as Tx
Inner diameter	Same as Tx
Outer diameter	Same as Tx
Secondary	
Winding type	clockwise spiral
Number of turns	Same as Tx
Wire type	Same as Tx
Inner diameter	Same as Tx
Outer diameter	Same as Tx
Antenna	
Pole	Same as Tx
Sphere	Same as Tx

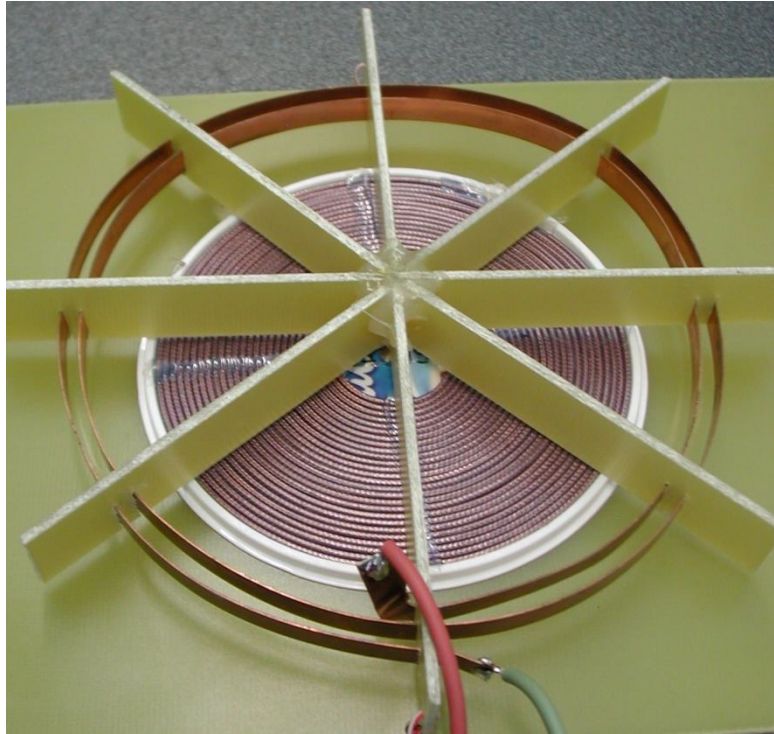Both helical coils (primary and secondary) are shown in the photograph (Fig.4).

Fig. 4

The first step: The generator output level is set approximately $2V$. The oscillator frequency is adjusted until the LED on the receiver will shine brightly. This corresponds to the resonance frequency f_{02} .

The above statements have been verified; in our experiment, as expected, the resonance frequencies f_{02} differ from experiment K. Meyl because of the size of the coils. The values found are: $f_{02} = 11{,}27 MHz$.

The second step: Grounding the receiver is disconnected. Then, the receiver LEDs turn off and the transmitter LEDs turn on again. Thus, as if the transmitter "feels" that the signal has been received by the receiver ("the reaction of the transmitter to the receiver"). The above statements have been verified.

In the third step we found the expected resonance at lower frequencies. The frequency found is: $f_{01} = 8{,}5 MHz$. Instead, the less clear "reaction" back on the transmitter at this lower frequency is not evident.

3.2 Discussion of the basic phenomenology

Phenomenon 1: The transmitter LED is "normally" on. (except in special circumstances). This behavior is easily explained, noting that the LED is in parallel with the same RF generator, so it is normally powered by the latter.

Phenomenon 2: By adjusting the frequency of the generator there is a value (8.5 *MHz*, see above) in which the receiver LED lights up. This effect is of course indicator of preferential transfer of energy from the transmitter to the receiver. The fact that this happens at a given frequency indicates the presence of a resonance, which in facts is verified instrumentally

with other methods, as mentioned below. If we increase the power of RF generator, the range of LED lighting widens as one would expect under the assumption of resonance.

The most important question is: which way energy is transmitted from the transmitter to the receiver? Two hypotheses can be proposed. The first one assumes that some sort of electromagnetic process is conveying the energy in the space between the spherical antennas. The features of such process are to be identified. Obviously, the usual capacitive coupling must be ruled out in this case, since this phenomenon, as mentioned below, is observed at large distances between the emitting and receiving antennas. In this sense, the radiating antenna is used as an energy source, and the receive antenna as an energy sink. But we cannot ignore, as a second hypothesis, that energy transfer can occur through the ground cable. We will carefully examine each of the assumptions made.

Phenomenon 3: At about the same frequency, or at least in a small range almost coincident, the Tx LED will turn off (or fade if the RF generator power is too high).

This effect is less intuitive. By use of instruments, we saw that the weakening of the signal on the transmitter LED is determined by the fact that the impedance seen at the transmitter primary - which is obviously a function of frequency - has a low value resistive component at the resonance frequency.

Phenomenon 4: When disconnecting the ground from the receiver, its light is extinguished and the transmitter LED goes on again.

Under the first of the hypothesis, this "reaction of the receiver on the transmitter" can be explained as follows: when disconnecting the receiver from ground, its reactance parameters changes and breaks the resonant mode of energy transfer between spherical antennas. As a result of sharply reduced level of energy absorbed by the receiver (the receiver LED goes off), the energy is no longer transferred from RF generator to the Tx, due to impedance mismatch; as a consequence more energy is available for the Tx LED (transmitter LED lights up).

The second hypothesis explains this phenomenon as the cessation of transmission of energy through the ground cable from its attachment to the receiver. For the same reason as above, the Tx LED have more energy again, and it lights up.

Phenomenon 5. Between the two spheres is inserted a grounded metal screen $(30 \times 40 cm)$. No significant attenuation of the received signal has been detected at both resonant frequencies. There is only a slight shift of the resonance frequencies.

If we assume that energy transfer occurs through a process between spherical wave antennas, it is necessary to conclude that it has properties different from properties of Hertzian waves. Again, this behaviour is compatible with the hypothesis of the signal transmission through the ground cable.

The experiments described above is not sufficient to unambiguously interpret the observed phenomena, and therefore have been produced additional experimental studies.

4. Additional experiments

4.1 Frequency response of the system

The availability of suitable laboratory equipment has allowed a detailed study of the global behaviour of the system in a frequencies range of 0-30MHz. For analogy with Meyl original resonance frequencies, in subsequent analysis we will refer to as f_{01} and f_{02} for the first and second resonance frequencies respectively, though the values will be somewhat different.

We used a Vector Network Analyzer (VNA) Agilent HP8753B and, equivalently, an Anritsu MS2026C, depending on laboratory availability.
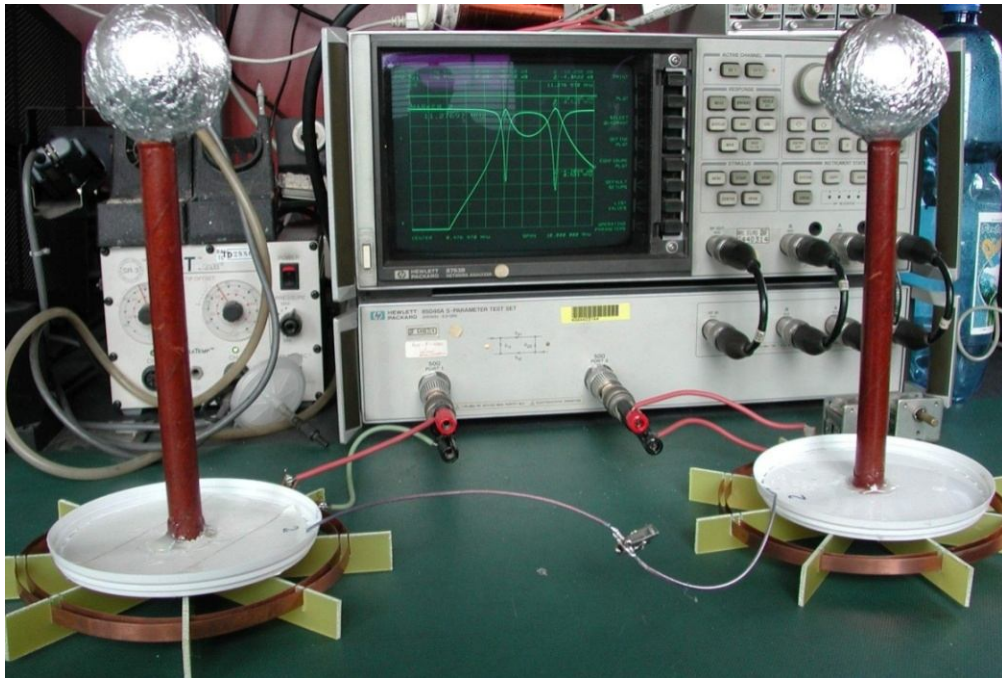

Fig. 5

The instrument was set in S_{21} mode, to display the frequency response of transmission from port 1 to port 2, and was calibrated. Port 1 of the VNA was then connected to the transmitter, and the output of the receiver was connected to port 2 of VNA (Fig.5). The transmission (from input to output) is characterized by the dimensionless (in decibels) S_{21} parameter, defined as:

$$S_{21} = 10 \cdot \log \frac{B_2}{A_1}.$$

where B_2 is the power wave outgoing from Port 2 and A_1 is the power wave incoming in Port 1.

The input reflection parameter, S_{11} is defined as:

$$S_{11} = 10 \cdot \log \frac{B_1}{A_1}.$$

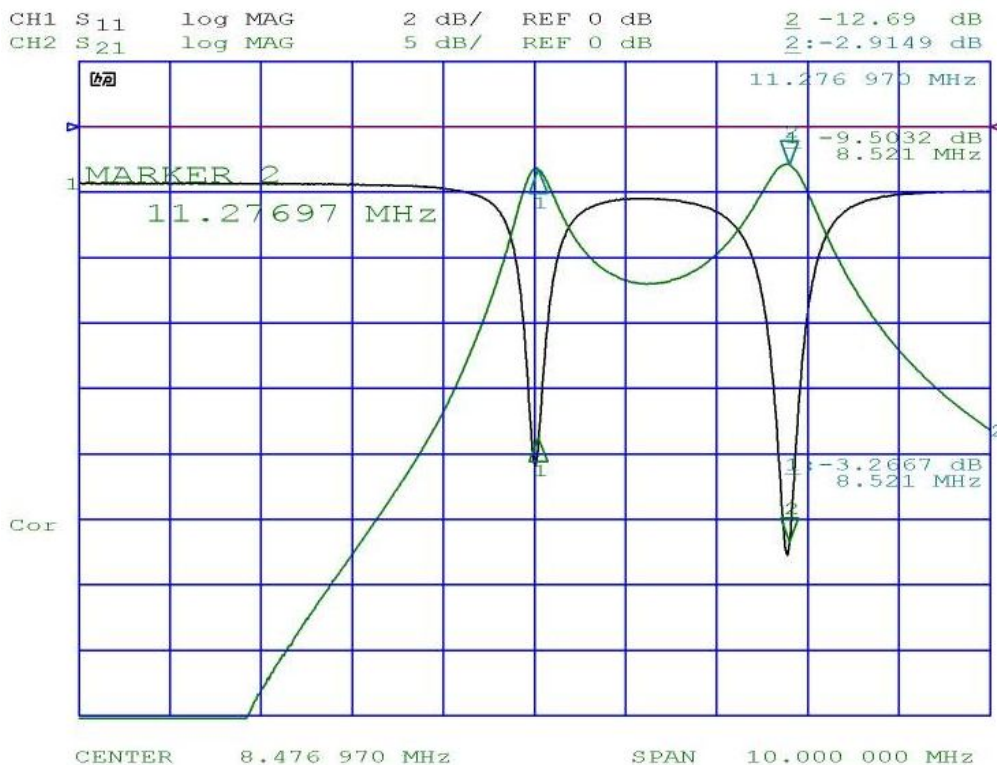where B_1 is the power wave reflected back from Port 1 and A_1 is the power wave incoming to Port 1.

Fig. 6

In the analysis of transmission amplitude-frequency characteristics, two resonances are visible (Fig. 6):
• the first at frequency $f_{01} = 8{,}52 MHz$ $(S_{21} = -3{,}2dB)$
• the second at frequency $f_{02} = 11{,}27 MHz$ $(S_{21} = -2{,}9dB)$.

Since, as mentioned, the black curve (S_{11}) describes (in decibels) the ratio of the power reflected back to the instrument's generator, over the forward power incident on the device input, a low value indicates low reflected power, therefore   much power transmitted to the device. As a consequence, this indirectly describes the current in the indicator circuit of the transmitter. It can

be seen, as expected, that each resonance minimum S_{11} also corresponds to the of the maximum energy released in the load receiver, as shown by trace S_{21}.

The peak value of the received signal at a frequency f_{01} is lower than the one at frequency f_{02}. This is consistent with the fact that Meyl notes: "By lowering the frequency of the signal indicator lights up the receiver again, but with less intensity."
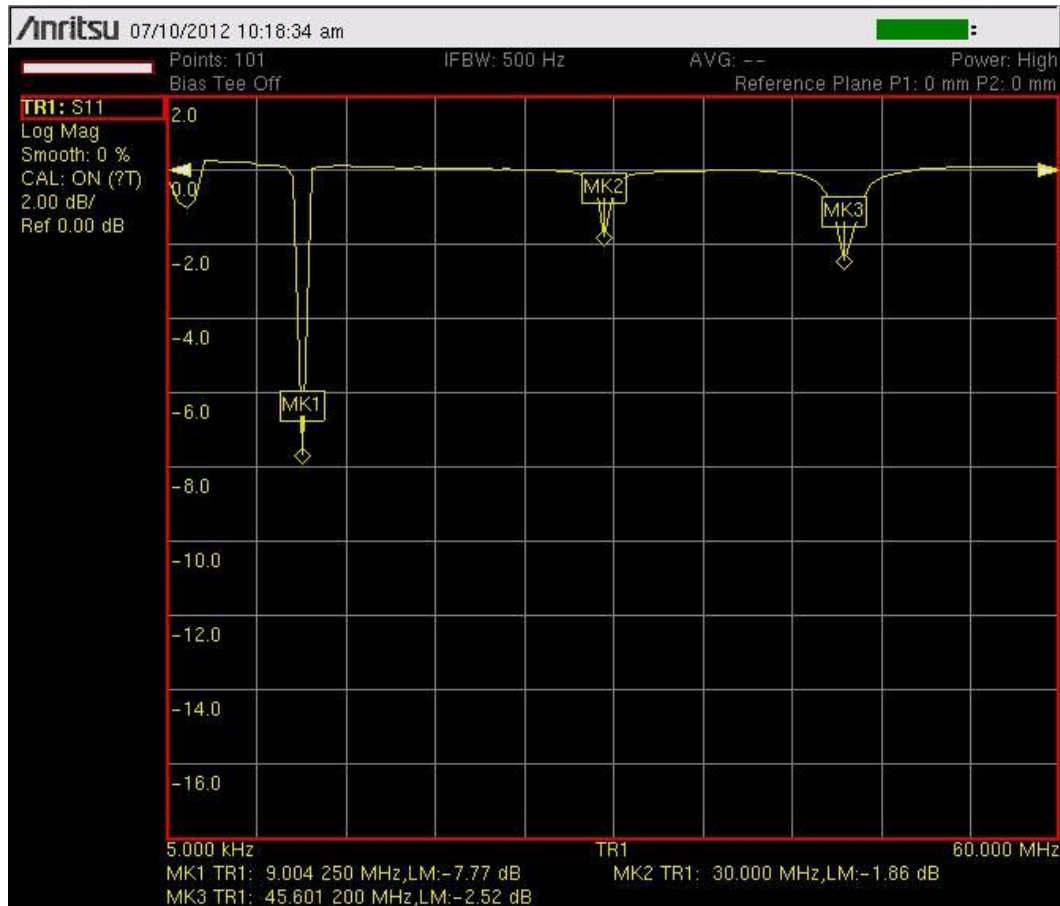

Fig. 7

The following experiment was performed with the *transmitter only* (the receiver being totally disconnected); we investigated the input reflection parameter, S_{11} versus frequency of the transmitter alone in the frequency range from 0 to 60 *MHz*. As visible in Fig. 7, three resonance peaks are present, at frequencies: $f_{01}^{(1)} = 9 MHz$ $\left(S_{11} = -7,77 dB\right)$, $f_{02}^{(1)} = 30 MHz$ $\left(S_{11} = -1,86 dB\right)$ and $f_{03}^{(1)} = 45,6 MHz$ $\left(S_{11} = -2,52 dB\right)$.

Obviously, comparing with the full system S_{11} behaviour (Fig. 6), the third peak is outside the frequency range and therefore not visible. In addition, we note that in an experiment with a solitary transmitter first resonance peak has shifted slightly, and the second resonant frequency is substantially increased. This means that the presence of the receiving system has a strong influence on the electromagnetic parameters of the process at a frequency of second

resonance peak. This again points to the distinguishing features between the electromagnetic processes occurring at different frequencies. It is also needed to explain the cause of resonance at the three frequencies where peaks occur.

4.2 Phase relationships at resonances

For this test, the complete system (transmitter and receiver) has been operated at a fixed frequency. Two probes of the oscilloscope (yellow and green lines in Fig.8a and Fig.8b) were placed at short distance (3-4cm) from the spheres, to sense the electric field. The third probe (blue trace) was close to the "ground" wire.

At $f_{01} = 8{,}52MHz$ (Fig.8a) signals on the transmitting and receiving antennas differ in phase by 180 degrees. The signal on the "ground" wire has an intermediate phase. Note its very low level.
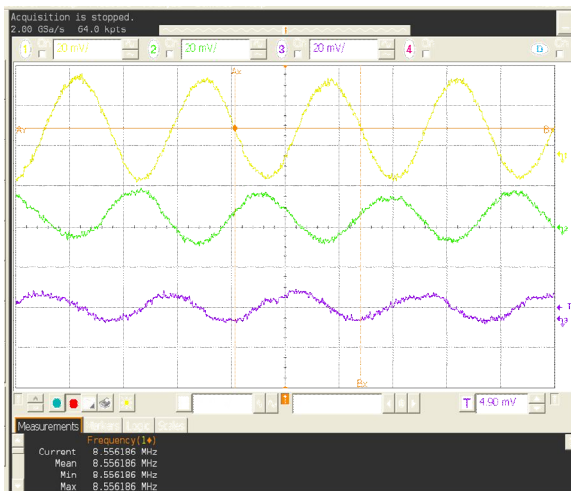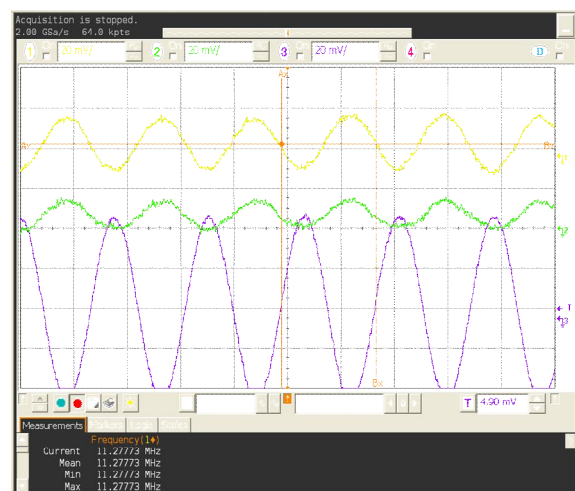

Fig. 8a   Fig. 8b

At $f_{02} = 11{,}27MHz$ signals on both antennas have the same phase (Fig. 8b). The signal in the "ground" wire is in counter-phase, and its level is very high.

All this confirms that the electromagnetic process at each resonant frequency has its own distinctive features.

4.3 Interpretation of the behaviour at the resonances

The above results are consistent with the model of the wire dipole antenna. For the resonance at $f_{01} = 8{,}52MHz$, in a dipole antenna with size equal to half the wavelength, (without any extra inductance and capacitance) the canonical voltage distribution is the one shown in Fig.9a.

In the presence of capacitive elements at the ends (Top loaded antenna dipole or Hertzian dipole), the geometric length of the dipole is reduced for the same resonance (Fig.9b). By adding an inductive load (Fig.9c) the geometric length of a dipole at the same resonance, is further reduced. From this diagram we see that:

- on the inductor, there is a jump of the charge (as well as potential);
- the terminal points of the dipole have potentials of opposite sign: they oscillate in opposite phase, as in the experimental waveform in Fig. 8*a*;
- the voltage in the middle point is theoretically zero (undefined phase, then), in good agreement with observed very low voltage on the "ground wire" (waveform of Fig. 8*a*, purple trace). Since the magnitude is nominally zero, the phase is unimportant here.
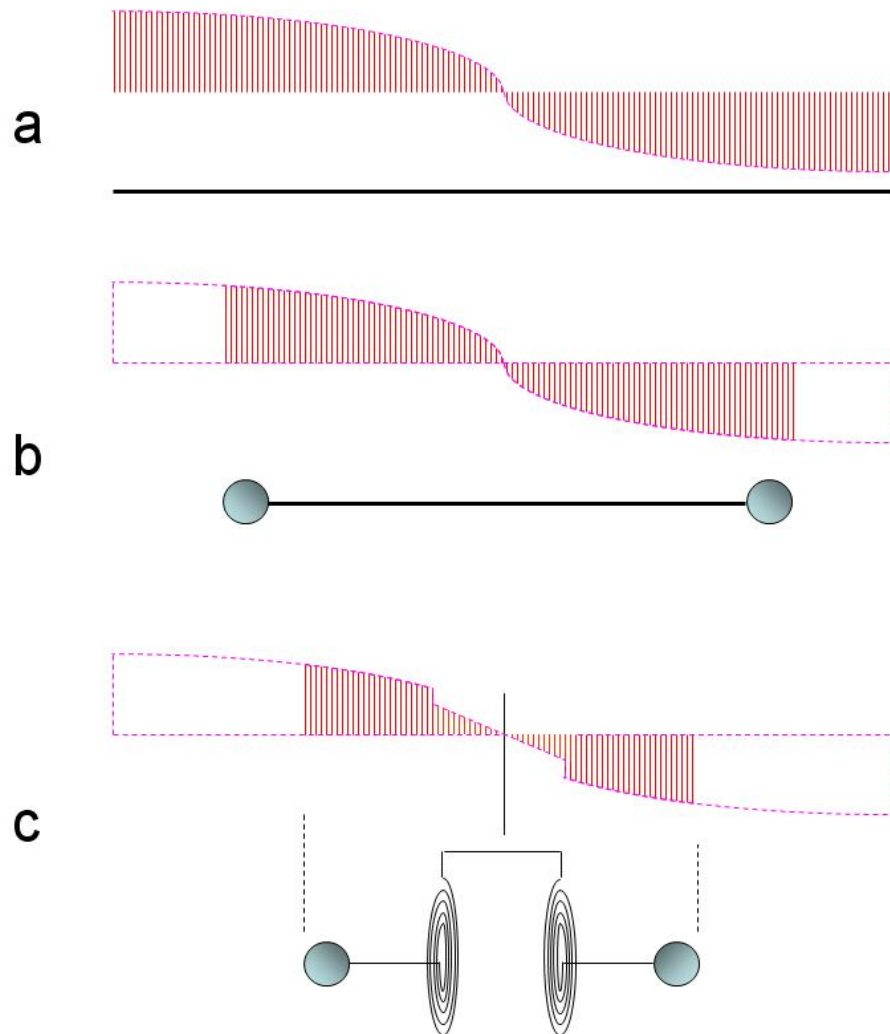

Fig. 9

We now consider the next resonance frequency (second overtone, $f_{02} = 11,27 MHz$). A common $\lambda / 2$ dipole would have the voltage distribution of Fig.10*a*. The capacitive load at the ends (Top loaded antenna dipole or Hertzian dipole) shortens the geometric length the dipole at the same resonance as shown in Fig.10*b*. The same considerations already mentioned apply. When adding an inductive load (Fig.10*c*), the geometric length of the dipole for the same resonance is further reduced. From this diagram we see that:

- on the inductor, there is the jump of the charge, as above, which leads to considerable increase of the voltage;

- the ends of the dipole have the same potential, therefore they oscillate in-phase (in agreement with Fig.8*b*, yellow and green traces);
- in the middle point the potential is very high and is in antiphase with respect to end potentials (as experimentally observed: Fig.8*b*, purple trace).
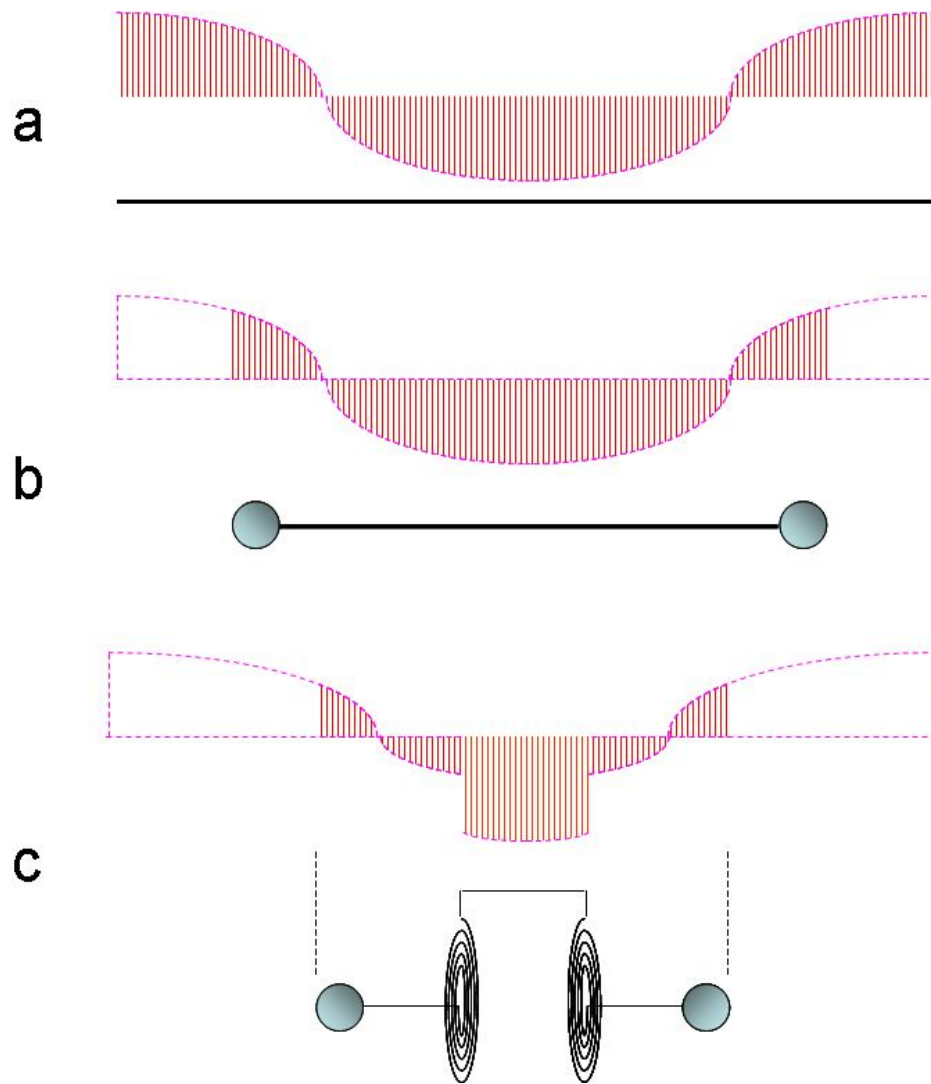
Fig. 10

4.4 Upper resonances in the individual Tesla Coil

An attempt has been made to visualize the resonances of the basic Tesla Coil (solitary transmitter) on a wider frequency range: 0 to 300*MHz*.

In order to avoid spurious resonances from the feeding cable itself, three EMI-type (dissipative) ferrite toroid cores have been inserted on the cable.

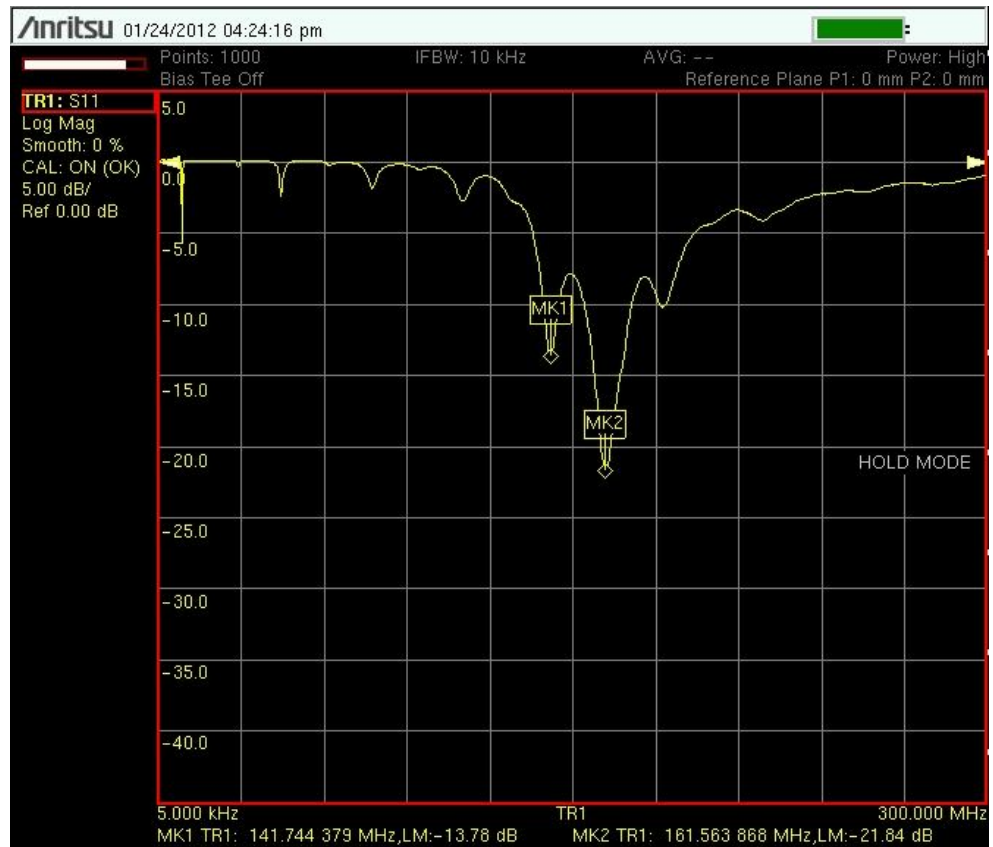Fig. 11

Fig. 12

The frequency response of energy absorption (Fig. 11) shows that the main resonance occurs near 160 *MHz* and has three peaks at frequencies $f_1 = 141{,}7 MHz$ [Marker 1], $f_2 = 161{,}5 MHz$ [Marker 2], and $f_3 = 179{,}8 MHz$

[Marker 3]. The observed initial response in the short wave is obviously not the main, the waveform shown on the left it shows the first peak.

4.5 Transmission loss versus distance

This series of tests studied the trend in the attenuation of the signal versus the distance between the transmitter and receiver. The transmitter and receiver were placed on wooden pedestals. They could be moved in the corridor of the building. The VNA analyzer was placed near the receiver. A 20-meter long coaxial cable (RG213, 50 *Ohm*) has been used to connect the VNA output to the transmitter. The "ground wire" had a length of 20 *m* too. Both cables length were not changed during the experiment[3].

4.5.1 Test at a distance 1 m

At 1-meter antennas distance the resonance peaks shifted somewhat compared with the previous bench tests, in which the distance between the antennas was less than 50 cm. As expected, the ground wire length of 20 *m*, extending from the transmitter to the analyzer, affects the resonant frequency, reducing it: $f_{01} = 7,9 MHz$, $f_{02} = 8,7 MHz$, $f_{03} = 10,8 MHz$. Attenuation at this frequency $f_{02} = 8,7 MHz$ is approximately $S_{21} = -3,8 dB$.

4.5.2 Test at a distance 4 m

Losses at resonance $f_{02} = 8,7 MHz$ of slightly increased: $S_{21} = -4,4 dB$ (Fig.13).

Fig.13

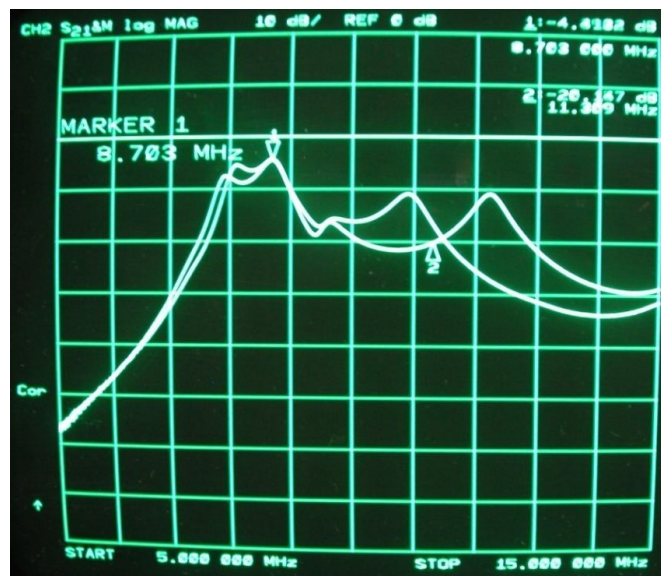[3] Note that, with respect to theoretical analysis (section 5.6 below) the resistance R_O would increase only with additional cable added; the resistance $R_{\rightarrow}$ remains unchanged. The obvious result is the relation: $R_O > R_{\rightarrow}$

It was observed that the frequency response significantly depends on the position of the grounding cable. Two tracks on the oscilloscope screen are examples of two different provisions of the grounding cable. The only unchanged point is the one corresponding to frequency 8.7MHz. An explanation of this fact is given in the theoretical analysis section below.

4.5.3 Test at a distance 15 m

The degree of attenuation at the resonant frequency $f_{02} = 8,7MHz$ (marker 1) remains unchanged: $S_{21} = -4,4dB$. At off-resonance frequencies, on the contrary, there are significant attenuations of the signal (Fig.14). (Note: vertical scale is 5dB per division). The second trace (memorized) is the previous test, for comparison.
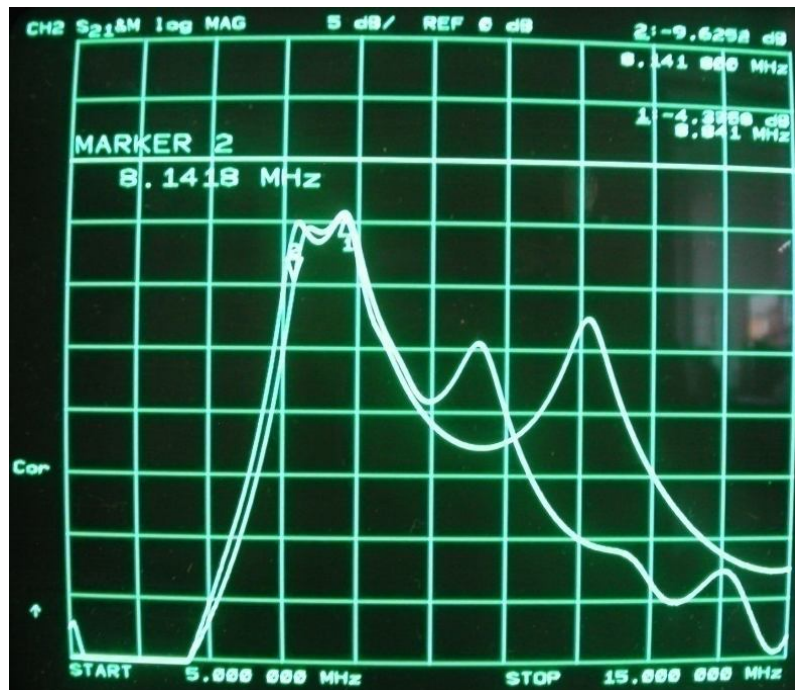

Fig. 14

4.5.4 Test at a distance 18 m (Through concrete wall)

In this test the line of sight was blocked by a concrete wall (Fig.15). Compared with the previous test, no difference has been observed: the resonance frequency $f_{02} = 8,7MHz$ the path loss remains the same: $S_{21} = -4,4dB$.

Fig. 15

The observed dependence of the attenuation at $f_{02} = 8,7 MHz$ versus distance is summarized in the table below:

Distance [m]	Path loss [dB]
1	-3.8
4	-4.4
15	-4.4
18	-4.4

At a distance of over $4m$ energy of the transmitted signal at a frequency $f_{02} = 8,7 MHz$ is stabilized. Such a decay law of the received signal as a function of the distance between the transmitter and the receiver is anomalous.

As noted above, in the experiments on signal transmission between the spherical antenna done by C. Monstein and J. P. Wesley [4], the transmitted signal faded as the square of the distance from the radiation source. Such dependence is a normal distribution with a spherical electromagnetic wave.

In contrast to C. Monstein and J. P. Wesley set-up, here the Tesla and K. Meyl antenna contain spiral coil. Perhaps the anomalous decay law of the signal energy due to processes occurring in the Tesla transformer. This phenomenon requires further study.

4.6 Transmission through a Faraday Cage

In the analysis of the observed phenomena it has been repeatedly raised the question: *is the energy transmitted from the transmitter to the receiver solely on ground conductor*? In other words: *is there a signal (energy) transmission path directly between the spherical antennas by electromagnetic waves*? And what

are the properties of these waves? It has been therefore tried to analyze this phenomenon more accurately using a professional Faraday cage (Fig.16).

Fig. 16

The transmitter was placed in the Faraday cage, mounted on a wooden table, and it was fed from the outside (VNA, port 1) by a coaxial cable through the cage connectors panel.

Fig. 17

The receiver was placed outside the cage on a wooden pedestal. The received signal was fed to the VNA analyzer port 2 (Fig.17).

4.6.1 Case1: ground cable is insulated

In the first test the ground wire from the transmitter was brought outside the cage through a small insulated hole in the metal wall (Fig. 18). The hole was about 8 mm in diameter, that is much smaller than the wavelength, so it should not affect the shielding of radiated signals.
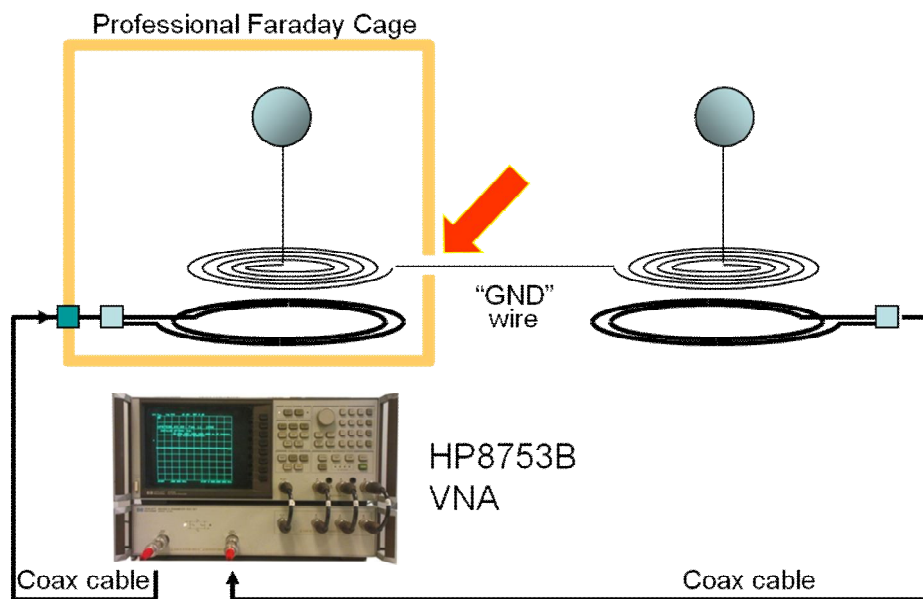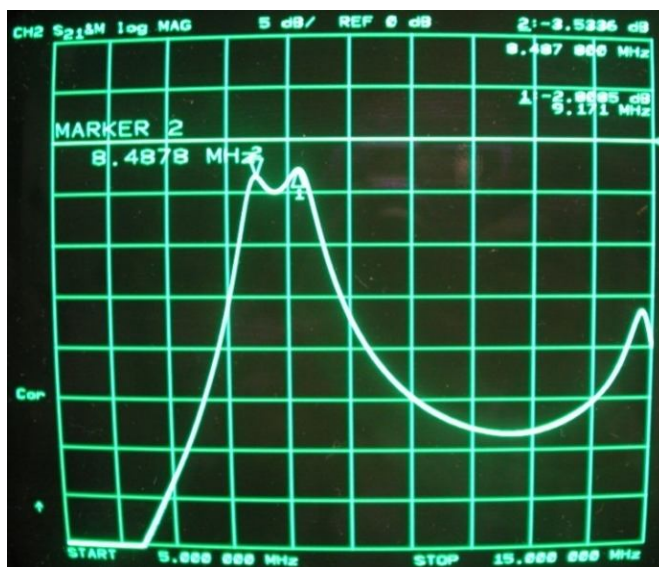
Fig. 18

Fig. 19

The cage door was first kept open, the transmitter and receiver being in the line of sight. Then, under the same conditions above the chamber door was closed.

Surprisingly, no difference was found: in Fig. 19 the two curves (with the door open and door closed) are identical, perfectly overlaying.

4.6.2 Case2: ground wires connected to the Faraday cage

The experiment was repeated with the same configuration as above, but the ground wire of the transmitter was electrically connected to the inner side of the cage metal wall, and the ground wire of receiver to the outer side of the cage metal wall (Fig. 20).
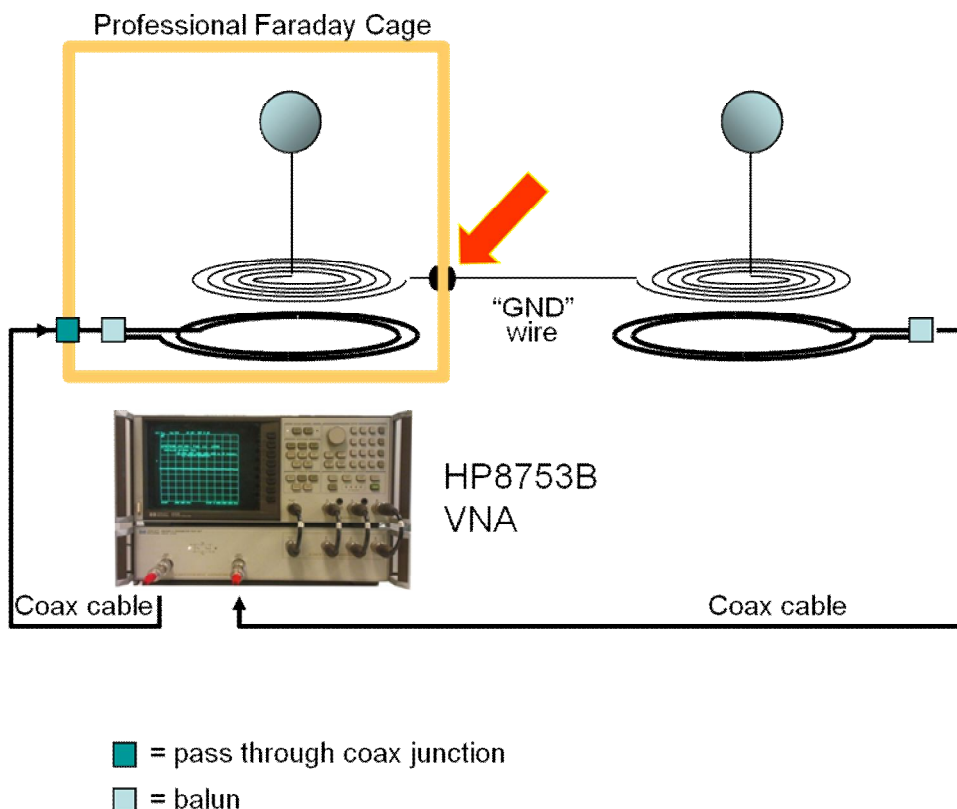
Fig. 20

Under these conditions, as before, there should be no obstacle on the ground conductor for a signal transmission from the transmitter to the receiver. However, in this case, the attenuation of the signal was found very high (high shielding effectiveness).

5.Theoretical analysis

To better understand the phenomena observed in the above experiments, it is necessary:
   • *to investigate the electromagnetic processes that take place between the transmitter and the receiver and find out their features;*
   • *explore the possibility of transmission of the signal (energy) over great distances.*
   • to *find out a theoretical model able to describe the resonances observed;*

From the standpoint of the modern theory of electromagnetic waves, the results of the experiments described above seem quite paradoxical. The

observed phenomena are obviously beyond the traditional concepts of the electromagnetic process. Hereafter we will refer to the generalized (four-) electrodynamics [7-9], which, as we will see, covers a wider range of phenomena.

5.1 The wave equations

In the macroscopic description, the theory of electrodynamic processes reduces to the well-known wave equations for the four-dimension vector-potential $(\mathbf{A}, \varphi)$:

$$\Delta \mathbf{A} - \varepsilon\mu \frac{\partial^2 \mathbf{A}}{\partial t^2} = -\mu\mathbf{j}, \tag{1}$$

$$\Delta \varphi - \mu\varepsilon \frac{\partial^2 \varphi}{\partial t^2} = -\frac{\rho}{\varepsilon}, \tag{2}$$

where ε and μ are respectively the dielectric permittivity and magnetic permeability, $\mathbf{j}$ and ρ are the current density and charge density.

Introducing the four-dimensional space-time,

$$x_1 = x, \quad x_2 = y, \quad x_3 = z, \quad x_4 = ict$$

we can write the corresponding components of the vector potential as

$$\Phi_1 = A_x, \quad \Phi_2 = A_y, \quad \Phi_3 = A_z, \quad \Phi_4 = ic\varphi,$$

and the four-wave equation that combines (1) and (2):

$$\Box\Phi_\nu = -\mu s_\nu, \quad (\nu = 1,2,3,4). \tag{3}$$

Here $\Box$ - is the invariant d'Alembert operator, and it is used a four-component current density vector:

$$s_1 = \rho V_x, \quad s_2 = \rho V_y, \quad s_3 = \rho V_3, \quad s_4 = ic\rho.$$

Let us consider the resulting four-dimensional divergence of the vector-potential:

$$\frac{\partial \Phi_1}{\partial x_1} + \frac{\partial \Phi_2}{\partial x_2} + \frac{\partial \Phi_3}{\partial x_3} + \frac{\partial \Phi_4}{\partial x_4} = div\mathbf{A} + \varepsilon\mu \frac{\partial \varphi}{\partial t}. \tag{4}$$

Typically, from mathematical considerations, this expression is assumed to be equal to zero, that is, it is apply the Lorentz condition. Disadvantages of this

approach are shown in the studies [7-9]: it is proposed to abandon the terms of Coulomb and Lorentz and assume the relationship:

$$B^*(x,y,z,t)=-div\mathbf{A}-\varepsilon\mu\frac{\partial\varphi}{\partial t}, \tag{5}$$

where $B^*(x,y,z,t)$ is a scalar function that characterizes an additional component of the magnetic field. In the stationary case:

$$B^*(x,y,z)=-div\mathbf{A}. \tag{6}$$

In the publications [7-9] it is theoretically and experimentally shown that the potential (scalar) component B^* of the magnetic field has a full physical meaning. Also discussed are the conditions under which there is a potential magnetic field. It is shown that the electric current in presence of an external potential magnetic field, experiences a force directed along the current or against it, depending on the sign of function $B^*(x,y,z)$. In said publications the irrotational law of electromagnetic induction is theoretically and experimentally substantiated: it is shown that in a conductor placed in a time-dependent potential magnetic field it is induced an electric field potential.

It follows that, for a complete description of the magnetic field it is required to use the four-vector $\left(\mathbf{B},B^*\right)$, which reflects its potential-vortex character. Thus, failure of Coulomb calibration, allows to consider both potential and vortex components of the vector $\mathbf{A}$. This implies a generalized field theory. We formulate the fundamental theorem of Helmholtz (Stokes) [12] applied to the vector $\mathbf{A}$: *if the divergence and the curl of the field, vanishing at infinity, is defined at each point $\mathbf{r}$ in a certain region, then everywhere in this region the vector $\mathbf{A}$ field can be uniquely represented as the sum of potential and solenoidal fields*:

$$\mathbf{A}=\mathbf{A}_\rightarrow+\mathbf{A}_O.$$

5.2 Electrodynamic properties of the vector potential

Usually the Helmholtz theorem is not directly applied to the vector magnetic potential $\mathbf{A}$, because the latter is considered just a support function and it is not uniquely determined. Let us examine the properties of the vector $\mathbf{A}$. In classical electrodynamics are used the following equations:

$$\mathbf{B} = rot\,\mathbf{A}, \qquad \mathbf{E} = -\frac{\partial\mathbf{A}}{\partial t} - grad\varphi. \tag{7}$$

and typically it is used the following gauge transformation:

$$\mathbf{A}' = \mathbf{A} + grad\chi, \quad \varphi' = \varphi - \frac{\partial \chi}{\partial t}, \tag{8}$$

where χ - is an arbitrary scalar coordinate-time function. The characteristics of the vortex magnetic field, $\mathbf{E}_O, \mathbf{D}_O$ and $\mathbf{B}, \mathbf{H}$ of the induced electric fields, are invariant under the transformation (8). On this basis it is concluded the gauge invariance of the electromagnetic field. This is the basis for the introduction of the Coulomb gauge and Lorentz condition. No physical meaning to the transformation (8), is usually, not given.

Let us try to explain physical meaning of gradient transformation. Note that by adding $grad\chi$ to the vector potential, its potential part changes. Potential part of a vector field changing without vortex component's changing is possible only in the transition from conventional fixed reference frame K to a steadily moving reference frame K'. But in this case, obviously, potential part of the electric field in the direction of the reference system must change. In moving reference frame the electric field of a point charge is not spherically symmetric, but appears Heaviside ellipsoid [13]. To compensate this change ("deformation"), an additive $\frac{\partial \chi}{\partial t}$ with a minus sign is introduced to the second correlation. Does the scalar potential φ really change at the transition from K to K'? It is known [13] that the charge is relative invariant value. Scalar potential φ depends on the location of the point of its definition and the magnitude of the charge, therefore, there is reason to consider it in all reference frames the same (at K' speeds much smaller than the speed of light). "Deformation" of the electric field in the transition to the mobile reference system is fully taken into account by vector potential $\mathbf{A}$. That is, there is no need to introduce a second correlation (8), it has no physical meaning. To describe the transformation of the electric field in the transition between K and K' (gradient transformation) only the first relation (8) is necessary.

There are two types of transformations of the vector field $\mathbf{A}$: gradient and vortex. Gradient transformation, as has been shown above, corresponds to the transition between progressively moving reference frames (one of them can be considered relatively immobile). When vortex transform, corresponds to a transition from progressively moving (or conditionally stationary) reference frame K to the rotating K'.

It can be shown rigorously [7] that upon gradient transformation the potential characteristics of the electromagnetic field ($\mathbf{A}_\rightarrow$, and, consequently, $\mathbf{E}_\rightarrow$ and B^*) will change, while vortex characteristics ($\mathbf{A}_O$, and, consequently $\mathbf{E}_O$ and $\mathbf{B}$) are invariants. Upon vortex transformation, on the contrary, vortex components of the electromagnetic field do change, and potential ones are invariants. This corresponds to the relative nature (depending on the choice of the reference frame) of the magnetic field and its basic characteristics -

vector $\mathbf{A}$: in other words, the correlation of solenoidal and potential components of the electrodynamic vector $\mathbf{A}$ depends on the choice of the reference system, but in the selected reference frame is uniquely determined. Information contained in brackets in the Stokes-Helmholtz theorem, merely reflects the relative character of motion (rest) of any reference system. In selected arbitrarily fixed reference frame it is convenient this vector constant equal to zero. In this approach, the ambiguity of the choice of potentials $\mathbf{A}$ and φ disappears, and there is no need to introduce gauge conditions. A theory formed on this platform will be called generalized electrodynamics.

5.3 Modified (generalized) Maxwell's equations

From wave equations (1) and (2) with the relations (5) and (7) we can easily obtain the *generalized equation of electrodynamics (Maxwell's modified equations)* [7-9]:

$$rot\mathbf{H} + gradH^{*} = \mathbf{j} + \frac{\partial \mathbf{D}}{\partial t} , \qquad (9)$$

$$div\mathbf{D} = \rho + \varepsilon'\varepsilon_0 \frac{\partial B^{*}}{\partial t} . \qquad (10)$$

This approach does not allow to exclude from these equations the potential (scalar) component of the magnetic field, which is described by two interrelated scalar functions:

$$B^{*} = \mu H^{*}. \qquad (11)$$

To denote the components of the magnetic field will use hereafter the term "scalar magnetic field" (SMF).

The equations of the generalized electrodynamics (9) - (10) take account of two non-stationary process: bias current $\frac{\partial \mathbf{D}}{\partial t}$ and $\varepsilon'\varepsilon_0 \frac{\partial B^{*}}{\partial t}$, which can be called "Charge-shift". The presence of a charge-shift due to the phenomenon of irrotational electromagnetic induction, has been confirmed experimentally [7]. Its essence is that of an unsteady SMF-induced electric field potential. Hence, a "quasi charge".

Another two differential equations that complement the generalized electrodynamics, are (7):

$$rot\mathbf{E} = -\frac{\partial \mathbf{B}}{\partial t} , \qquad (12)$$

$$div\mathbf{B} = 0 . \qquad (13)$$

Equation (12) describes the phenomenon of electromagnetic eddy induction. In Maxwell's electrodynamics we consider only the eddy time-dependent processes. The generalized electrodynamics describes, in addition,

time-dependent processes that give rise to the potential components of electric and magnetic fields. If these transients are created by third-party generators, they are the real sources of the electromagnetic field. Instead, in the case of the free field at any given point in time should be considered as quasi sources.

Equations (9) - (10), (12) - (13) and of their individual functions describe electromagnetic phenomena, and for a complete description of the electrodynamic processes we must also use the wave equation (1) - (2) and the main electrodynamic characteristics, the 4- dimensional vector potential $(\mathbf{A}, \varphi)$.

In papers [7-9], the potential component of the magnetic field was studied theoretically and experimentally. A particularly useful formula (14) allows to determine the intensity of the SMF, the created by the current J of finite length (Fig. 21):

$$H^*(x',y',z') = \frac{J}{4\pi} \int_0^L \frac{z\,dz}{r^3} = \frac{J}{4\pi} \frac{(r_1 - r_2)}{r_1 r_2} = \frac{J}{4\pi r_0}(\sin\alpha_2 - \sin\alpha_1). \tag{14}$$
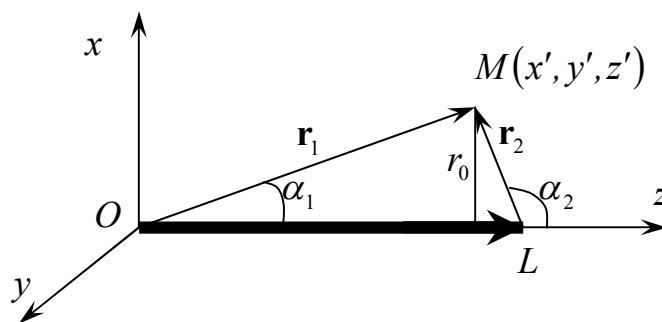

Fig. 21

In Fig. 22 presents the line of the vector potential $\mathbf{A}$ and magnetic field vector $\mathbf{H}$ and scalar magnetic field H^* created by a straight current segment of finite length.
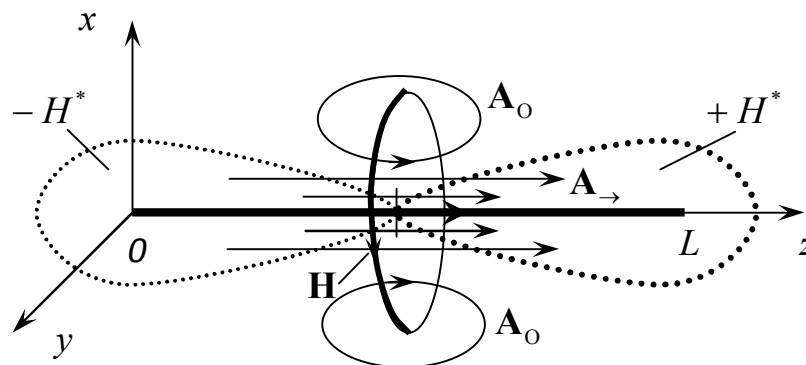

Fig. 22

Based on the results of studies [7-9], we can formulate the rule: *looking from the midpoint of a finite-length current element, towards the direction of current flowing in it, it is created a positive SMF ahead, and a negative SMF behind.* Note that the SMF in its essence is always heterogeneous and spatially unrestricted (i.e., it vanishes at infinity).

5.4 Wave processes

From equations (1) - (2) using the second relation (7) we can easily obtain the wave equation:

$$\Delta \mathbf{E} - \mu\varepsilon \frac{\partial^2 \mathbf{E}}{\partial t^2} = \mu \frac{\partial \mathbf{j}}{\partial t} + \frac{1}{\varepsilon} grad\rho . \tag{15}$$

Conduction currents can be separated into radial $\mathbf{j}_\rightarrow$ and azimuthally $\mathbf{j}_O$ components. With this in mind, it is now possible to split (15) into two independent equations:

$$\Delta \mathbf{E}_\rightarrow - \mu\varepsilon \frac{\partial^2 \mathbf{E}_\rightarrow}{\partial t^2} = \mu \frac{\partial \mathbf{j}_\rightarrow}{\partial t} + \frac{1}{\varepsilon} grad\rho , \tag{16}$$

$$\Delta \mathbf{E}_O - \mu\varepsilon \frac{\partial^2 \mathbf{E}_O}{\partial t^2} = \mu \frac{\partial \mathbf{j}_O}{\partial t} . \tag{17}$$

Similarly, using the first relation (7) from (1) - (2), we obtain the wave equation for the vector $\mathbf{H}$:

$$\Delta \mathbf{H} - \varepsilon\mu \frac{\partial^2 \mathbf{H}}{\partial t^2} = -rot\mathbf{j}_O . \tag{18}$$

Equations (17) and (18) describe the well-known mechanism of the emission of transverse electromagnetic waves.

Similarly, transforming (1) - (2) with (6), we obtain the wave equation for a scalar function H^* :

$$\Delta H^* - \varepsilon\mu \frac{\partial^2 H^*}{\partial t^2} = \frac{\partial\rho}{\partial t} + div\mathbf{j}_\rightarrow . \tag{19}$$

The differential equations (16) and (19) together describe the propagation of waves along the irrotational vector $\mathbf{E}_\rightarrow$, so they should be called the *longitudinal* or *electroscalar* [10, 15].

It is important to note that, since the vortex and potential components of the corresponding fields are mutually independent, equation (16) - (19) are fully consistent with the principle of superposition. The sources generating potential and vortex fields are respectively separated. However, there is a question of mutual communication between non-closed conduction currents and charges,

which reflects the condition of continuity. In Maxwell's electrodynamics is used as a continuity condition:

$$\frac{\partial \rho}{\partial t} + div\mathbf{j}_{\rightarrow} = 0 . \tag{20}$$

Let's write the differential equation (10) in the form:

$$div\mathbf{D} = \varepsilon'\varepsilon_0 \frac{\partial B^*}{\partial t}.$$

After differentiation in time, we get:

$$\varepsilon'\varepsilon_0 \frac{\partial^2 B^*}{\partial t^2} - div\frac{\partial \mathbf{D}}{\partial t} = 0. \tag{21}$$

As a result of the addition (20) and (21), we obtain the more *general condition of continuity*:

$$\frac{\partial \rho}{\partial t} + \varepsilon'\varepsilon_0 \frac{\partial^2 B^*}{\partial t^2} + div\left(\mathbf{j} - \frac{\partial \mathbf{D}}{\partial t} \right) = 0.$$

Therefore, current sources can be created without the help of non-stationary charges, but by alternating potential magnetic field. In this sense, the usual electric charges and their currents become independent from conductance.

Let us write down the equation of continuity in three particular cases.

•As a first case, assume an unsteady SMF (variable not electric charges) is present in some point of a conductive medium; then

$$\varepsilon'\varepsilon_0 \frac{\partial^2 B^*}{\partial t^2} + div\mathbf{j}_{\rightarrow} = 0.$$

That is, if a given point of an (insulated) conductor is exposed to a transient SMF $\left(\frac{\partial^2 B^*}{\partial t^2} \neq 0 \right)$, then a current transient occurs. This phenomenon can be used for receiving signals transmitted by electroscalar waves.

•As a second case, a dielectric body is exposed to a transient SMF. The continuity equation is in the form (21). That is, in the absence of a conductive environment, only bias current occurs.

•As a third case, let us consider conducting and non-conducting regions exposed to the SMF; the continuity equation is:

$$\varepsilon'\varepsilon_0 \frac{\partial^2 B^*}{\partial t^2} + div\left(\mathbf{j}_{\rightarrow} - \frac{\partial \mathbf{D}_{\rightarrow}}{\partial t} \right) = 0 \tag{22}$$

This is the case in a spiral coil: conductive and dielectric sites are radially alternated.

In conclusion, from the all above considerations it can be affirmed that *the state and evolution of the electromagnetic field in a macroscopic approximation to the selected coordinate system is uniquely described by the four-dimensional vector* $(\mathbf{A}, \varphi)$*, including the potential and solenoidal components and satisfies the four-dimensional d'Alembert equation.* If we separate the potential and vortex part of the vector $\mathbf{A}$ in (1) - (2), then seven independent scalar differential equations containing seven mutually independent variables are obtained. All other characteristics of the electromagnetic field (intensity, induction) are secondary, they are uniquely expressed through the potential $(\mathbf{A}, \varphi)$.

A very similar position expressed in his article, K. J. van Vlaenderen [10]. The author of this article also pointed out the gauge conditions, as reasons for the limited and electrodynamic theory was modified equations, which coincide with (9) - (10) (12) - (13). However, he did not use the continuity equation in general form (21) and did not abandon gauge invariance in its traditional interpretation. This piecemeal approach has inherent contradictions. Therefore, Bruhn G. W. [16] expressed doubts about the validity of the theory, developed by K. J. van Vlaenderen.

Higher generalization of electrodynamics can be done at a quantum level, using two four-vector. Generalized equations of quantum electrodynamics led Hvorostenko N.P. [6], their analysis is contained in [7]. A similar result with regard to quantum processes was obtained by Dale A. Woodside [11].

5.5 The mechanism of radiation and propagation of the electroscalar waves

Let us try to clarify the mechanism of electroscalar waves radiation from ball shaped antennas. Equation (19) states that, due to changes in electric charge, an unsteady SMF $H^{*}(x, y, z, t - r/c)$ is generated.

Vector $grad\rho$ is directed radially in the area. In accordance with (16), it is formed around the sphere the radial electric field $\mathbf{E}_{\rightarrow}(x, y, z, t - r/c)$. Thus, the as an effect of a variable electric charge, it is generated an electroscalar wave, which is determined by the vector $\mathbf{E}_{\rightarrow}(x, y, z, t - r/c)$ and scalar function $H^{*}(x, y, z, t - r/c)$.

A previous experiment confirming the above theoretical considerations is described in the article [4], by the German researchers C. Monstein and J. P. Wesley. In said experiment ball antennas installed at a distance of 10 to 1000 m were used. The emitting antenna created a variable electric charge, and the receiving antenna could receive the signal those level was found to be proportional to the square of the distance from the radiation source.

Let us consider the propagation of electromagnetic waves in a fixed homogeneous dielectric medium, without charges:

$$\varepsilon' = const, \quad \mu' = const, \quad \sigma = 0, \quad \rho = 0.$$

Equations (9), (10), (13) in this case takes the form:

$$rot\mathbf{H} + gradH^* = \varepsilon'\varepsilon_0 \frac{\partial \mathbf{E}}{\partial t}, \tag{23}$$

$$rot\mathbf{E}_O = -\mu'\mu_0 \frac{\partial \mathbf{H}}{\partial t}, \tag{24}$$

$$div\mathbf{E} = \mu'\mu_0 \frac{\partial H^*}{\partial t}. \tag{25}$$

Equation (23) implies two independent equations:

$$rot\mathbf{H} = \varepsilon'\varepsilon_0 \frac{\partial \mathbf{E}_O}{\partial t}, \tag{26}$$

$$gradH^* = \varepsilon'\varepsilon_0 \frac{\partial \mathbf{E}_\rightarrow}{\partial t}. \tag{27}$$

That is, time-varying electric field generates eddy vortex magnetic field. A time-varying electric field generates a potential SMF. Consequently, these processes in the absence of conduction currents can be conventionally separated.

We differentiate (26) with respect to time:

$$rot\frac{\partial \mathbf{H}}{\partial t} = \varepsilon'\varepsilon_0 \frac{\partial^2 \mathbf{E}_O}{\partial t^2}.$$

Using equation (24), we obtain:

$$-\frac{1}{\mu'\mu_0} rotrot\mathbf{E}_O = \varepsilon'\varepsilon_0 \frac{\partial^2 \mathbf{E}_O}{\partial t^2}$$

arriving at the homogeneous D'Alembert equation for the vortex vector $\mathbf{E}_O$:

$$\Delta\mathbf{E}_O - \mu'\mu_0\varepsilon'\varepsilon_0 \frac{\partial^2 \mathbf{E}_O}{\partial t^2} = 0. \tag{28}$$

Similarly, considering simultaneously the equations (27) and (25), we obtain the wave equation for the vector potential $\mathbf{E}_\rightarrow$:

$$\Delta\mathbf{E}_\rightarrow - \mu'\mu_0\varepsilon'\varepsilon_0 \frac{\partial^2 \mathbf{E}_\rightarrow}{\partial t^2} = 0. \tag{29}$$

Differentiating (24) with respect to time:

$$rot \frac{\partial \mathbf{E}_O}{\partial t} = -\mu' \mu_0 \frac{\partial^2 \mathbf{H}}{\partial t^2}.$$

In view of (26), we obtain the equation for the vector of the d'Alembert $\mathbf{H}$:

$$\Delta \mathbf{H} - \mu' \mu_0 \varepsilon' \varepsilon_0 \frac{\partial^2 \mathbf{H}}{\partial t^2} = 0. \tag{30}$$

By a similar transformation equations (25) and (27) we arrive to the wave equation for a scalar function H^*:

$$\Delta H^* - \mu' \mu_0 \varepsilon' \varepsilon_0 \frac{\partial^2 H^*}{\partial t^2} = 0. \tag{31}$$

Thus, *the whole picture of an electromagnetic wave is constituted by the two components: one of them is determined by the vortex vectors* $\mathbf{E}_O$ *and* $\mathbf{H}$, *and other by a potential vector* $\mathbf{E}_\rightarrow$ *and a scalar function* H^*.

We note that the propagation velocity of longitudinal and transverse electromagnetic waves are the same:

$$V_\perp = V_\parallel = \frac{1}{\sqrt{\varepsilon' \varepsilon_0 \mu' \mu_0}} = \frac{c}{\sqrt{\varepsilon' \mu'}}, \tag{32}$$

where $c = \dfrac{1}{\sqrt{\varepsilon_0 \mu_0}}$ is the speed of light in vacuum. This expresses the inextricable connection between all components of the electromagnetic process and the inability to complete their positional separation in general. Moreover, the transverse electromagnetic waves propagating in a material medium, in every point in space generate longitudinal waves and vice versa.

5.6 Electromagnetic processes in the Tesla coil

5.6.1 Vortex and potential processes

First of all, we notice that in the original Tesla experiment, and consequently in the Meyl device, there is a fundamental difference from a normal radio component: in facts, the conventional transformers are usually based on solenoid coils, while Tesla adopts spiral coils. In a conventional transformer the electromagnetic induction phenomenon is based on the vortex, that is a mutual transformation of the vortex magnetic field. In a such transformer windings currents have circular (eddy) flow.
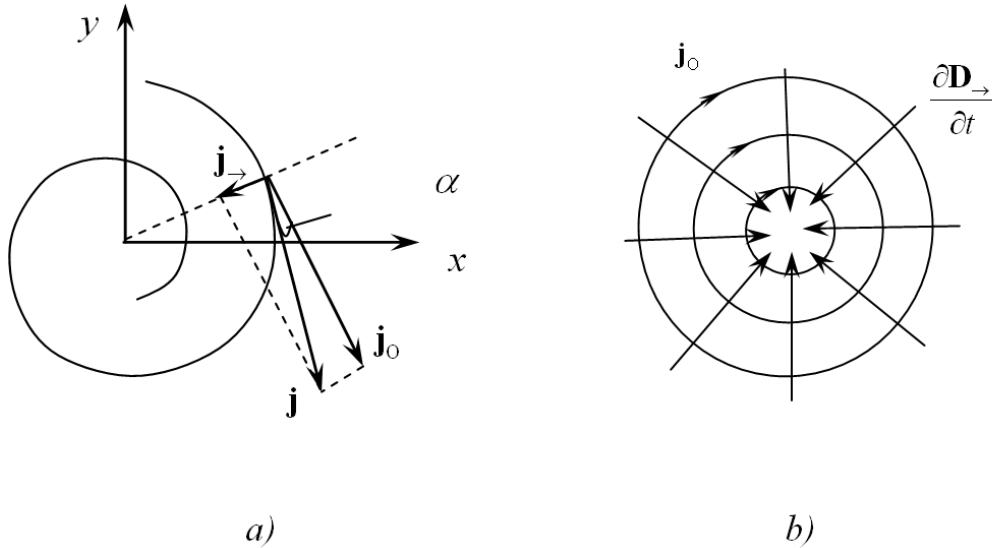
a)   b)

Fig. 23

Instead, Tesla transformer is designed so that there are two co-planar current components: the tangential (swirl) $\mathbf{j}_O$ and radial (irrotational) $\mathbf{j}_\rightarrow$ (Fig. 23*a*):

$$\mathbf{j} = \mathbf{j}_O + \mathbf{j}_\rightarrow .$$

Consequently, the electric field in the coil can be represented as a superposition of a *vortex* (solenoidal) component and a *potential* (irrotational) component:

$$\mathbf{E} = \mathbf{E}_O + \mathbf{E}_\rightarrow .$$

When describing the processes occurring in a helical coil, equation (9) can be split into two partial differential equations:

$$rot\mathbf{H} = \mathbf{j}_O + \frac{\partial \mathbf{D}_O}{\partial t}, \tag{33}$$

$$grad H^* = \mathbf{j}_\rightarrow + \frac{\partial \mathbf{D}_\rightarrow}{\partial t}. \tag{34}$$

Equation (33) describes an electromagnetic vortex process, while equation (34) describes an irrotational electromagnetic process. The time-derivative terms in the right parts of the above equations obviously vanish when the involved processes are stationary; in quasi-stationary (e.g. low frequency) cases, such time derivative terms can be neglected, with respect to current components $\mathbf{j}_O$ and $\mathbf{j}_\rightarrow$ respectively. From Fig.23*a* it is apparent that a geometric correlation between the current components magnitudes depending on the design of spiral coil (angle α); the related electric field components consequently has the same relationship:

$$tg\alpha = \frac{j_{\rightarrow}}{j_O} = \frac{E_{\rightarrow}}{E_O}. \tag{35}$$

Hence, equation (33), (34) in stationary and quasi-stationary case are usually linked by the ratio (35).

In non stationary case, when considering the electromagnetic process unfolding along the conductors of the coil, the current conductance $\mathbf{j}_O$ is usually strong, thus in equation (33) the Eddy displacement current $\frac{\partial \mathbf{D}_O}{\partial t}$ can be neglected. Moreover, the angle α in spirals is usually small, therefore $j_{\rightarrow} \ll j_O$. This suggests that in equation (34) the currents conductivity $\mathbf{j}_{\rightarrow}$ can be small enough to be neglected compared to current offset $\frac{\partial \mathbf{D}_{\rightarrow}}{\partial t}$. The latter term, obviously, gets more and more important as the involved frequency increases, as the time derivative increases accordingly. Thus, equation (33) and (34) are simplified as:

$$rot\mathbf{H} = \mathbf{j}_O, \tag{36}$$

$$gradH^* = \frac{\partial \mathbf{D}_{\rightarrow}}{\partial t}. \tag{37}$$

These differential equations are independent: the two electromagnetic process (Vortex and potential) in Tesla coil can be treated separately. In Fig 23*b* the tangential $(\mathbf{j}_O)$ and radial $\left(\frac{\partial \mathbf{D}_{\rightarrow}}{\partial t}\right)$ components of the current in the coil Tesla are depicted separately at a specific time instant.

5.6.2 The transformation mechanism

In the complete Tesla transformer with two spiral coils, two phenomena are occurring simultaneously: vortical electromagnetic induction and irrotational electromagnetic induction.

The *vortical* electromagnetic induction, as we know, results in the transformation of the Eddy currents. That is, in the secondary coil a conduction currents $\mathbf{j}_O(t)$ is developed.

Through *irrotational* electromagnetic induction a transformation of radial currents occurs. The radial conduction currents $\mathbf{j}_{\rightarrow}(t)$ in the primary coil, are transformed in the radial displacement currents $\frac{\partial \mathbf{D}_{\rightarrow}}{\partial t}$, that arise in the secondary coil.

Let us try to describe this process in more detail. A radial conduction current $\mathbf{j}_\rightarrow(t)$ in the primary coil creates a SMF gradient, according to equation (10). This gradient is parallel to the $\mathbf{j}_\rightarrow(t)$ current, so it is radial as well. Assuming the above currents, and thus SMF, are time dependent, in the Tesla coil secondary a radial induction is obtained, according the equation (21) due to changes in the SMF. This should be thought of as the motion of the displacement charge (*quasi charge*) $\varepsilon'\varepsilon_0 \dfrac{\partial B^*}{\partial t}$ in the radial direction. Such currents can be called *"displacement currents of the second type"* in contrast to Maxwell's displacement current $\dfrac{\partial \mathbf{D}_\mathrm{O}}{\partial t}$, which is obtained from Eddy current. Note that the displacement currents are transferred in the absence of an electrically conducting medium. Therefore, the isolation between the turns of the coil does not preclude the current $\dfrac{\partial \mathbf{D}_\rightarrow}{\partial t}$.

Radial displacement current leads to the separation of electric quasi-charges in the radial direction, between the centre and the periphery of the secondary coil, so that there is the gradient potential. The spherical radiating antenna connected to the centre of the coil, is then subjected to an unsteady electric potential. In turn, this creates a strong electric field around the spherical antenna. Such electric field is non-stationary, and has a radial structure characterized by a vector $\mathbf{E}_\rightarrow(x,y,z,t-r/c)$.

Let us consider a simplified model describing the mechanism of transformation of radial currents, as depicted in Fig. 24a. Consider two sections of the conductor, located on the same line. The left element models the radial current flowing in the primary coil, and the right element represents the one in the secondary coil.
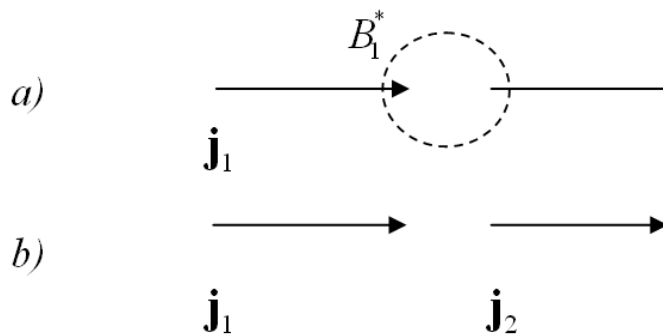

Fig. 24

Let the primary current varies as:

$$\mathbf{j}_1 = \mathbf{j}_{01}\sin\omega t. \tag{38}$$

As already described above in Fig. 22 and the accompanying analysis, in the space between the two aligned conductors the current $\mathbf{j}_1$ creates a time varying SMF (Fig. 24a) that can written as:

$$B_1^* = B_{01}^* \sin \omega t. \qquad (39)$$

Therefore, in this area will arises a transient effective charge:

$$\rho_{ef} = \frac{\partial B_1^*}{\partial t} = B_{01}^* \omega \cos \omega t.$$

In accordance with the continuity equation (21) in this region there is a current source:

$$div \frac{\partial \mathbf{D}}{\partial t} = \varepsilon' \varepsilon_0 \frac{\partial^2 B_1^*}{\partial t^2} = -\varepsilon' \varepsilon_0 B_{01}^* \omega^2 \sin \omega t. \qquad (40)$$

In the right conductor is developed the current of conduction:

$$div \mathbf{j}_2 = \varepsilon' \varepsilon_0 \frac{\partial^2 B_1^*}{\partial t^2} = \varepsilon' \varepsilon_0 B_{01}^* \omega^2 \sin \omega t. \qquad (41)$$

Thus, in the secondary coil a new current $\mathbf{j}_2$, flowing in phase with the primary current $\mathbf{j}_1$ is induced (Fig. 24b). With these considerations we have neglected the time delay, assuming that the conductors are located at a distance much smaller than the length of the corresponding wave.

In the first conductor, of course, there is a backflow (an analogue of the Lenz rules). Therefore, the primary current is somewhat weakened, and its energy reduced. It can be said that in this process energy is transferred from the primary to the secondary. This phenomenon explains the mechanism of separation of charges in a spiral coil.

Let's write the laws for the Vortex and an irrotational processes. For the vortex process, as widely known:

$$U_O = -L_O \frac{dJ_O}{dt}. \qquad (42)$$

To derive a similar formula, which describes the irrotational electromagnetic process we use equation (10) written in the form:

$$div\mathbf{D} = \varepsilon' \varepsilon_0 \frac{\partial B^*}{\partial t}.$$

As a result of integration with respect to the scope and application of the Gauss theorem, we determine the effective charge (the charge of bias) induced in the volume τ:

$$q_{\scriptscriptstyle{\ni\phi}} = \varepsilon'\varepsilon_0 \int_{\tau} \frac{\partial B^*}{\partial t} d\tau . \tag{43}$$

In the case of a flat coil, $d\tau = 2\pi r b \cdot dr$ where b - the diameter of the cable conductor (height coil). Hereafter, for simplicity, we'll consider $\varepsilon' = 1$.

According to equation (37) SMF in our case generates a radial displacement currents. We write (37) in cylindrical coordinates:

$$\frac{\partial H^*(r,t)}{\partial r} = j_{\rightarrow}^{dis}(r,t), \qquad \text{here} \qquad j_{\rightarrow}^{dis}(r,t) = \frac{\partial D_{\rightarrow}}{\partial t}.$$

Suppose that in all the turns of the coil, at a given time, the radial current has the same direction. This corresponds to the G. Wheeler approximation [14]. Displacement current density in this case varies depending on the radius with the law:

$$j_{\rightarrow}^{dis}(r,t) = \frac{R_0}{r} j_{\rightarrow}^{dis}(R_0,t).$$

Where R_0 is the coil radius at periphery.
From this relation, we obtain by integration:

$$H^*(r,t) = R_0 \ln|r| j_{\rightarrow}^{dis}(R_0,t),$$

or

$$B^*(r,t) = \mu_0 R_0 \ln|r| j_{\rightarrow}^{dis}(R_0,t). \tag{44}$$

Substituting (44) into (43), determined by the charge displacement occurs on the periphery of the coil (the same charge is formed on the inner coil of the coil):

$$q_{\scriptscriptstyle{\ni\phi}} = \mu_0 \varepsilon_0 \int_{r_0}^{R_0} r \ln|r| dr \cdot \frac{dJ_{\rightarrow}^{dis}(R_0,t)}{dt} .$$

In the above integration we have noted that the radial force of the bias current at the periphery of the coil is:

$$J_{\rightarrow}^{dis} = j_{\rightarrow}^{dis}(R_0,t) \cdot 2\pi R_0 b .$$

Thus, the spiral coil behaves as an analog of a cylindrical capacitor: in facts, as depicted in the following figure, radial bias current leads to charge

separation bias q^{dis} (Fig. 25). These charges create an electric field that seek to reduce the bias current. This is the physical essence of irrotational electromagnetic induction.
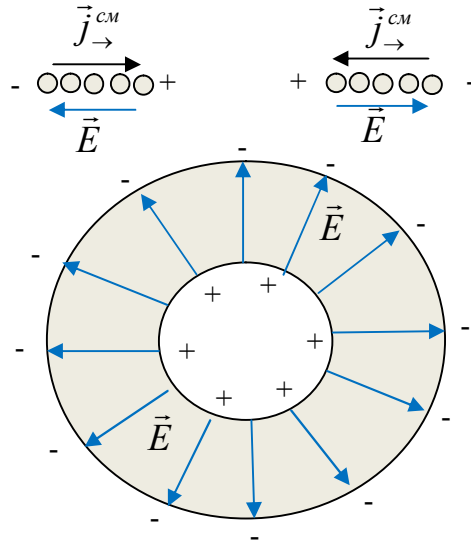

Fig. 25

Thus, the spiral coil is an analog of a cylindrical capacitor:

$$C_{\to} = \frac{2\pi\varepsilon_0 b}{\ln\left|\dfrac{R_0}{r_0}\right|}.$$

Since $q_{ef} = C_{\to} U_{\to}$, we obtain an analogue of the law (42):

$$U_{\to} = \frac{\mu_0}{2\pi b}\ln\left|\frac{R_0}{r_0}\right| \int_{r_0}^{R_0} r\ln|r|\,dr \cdot \frac{dJ_{\to}^{dis}(R_0,t)}{dt}. \qquad (45)$$

That is

$$U_{\to} = L_{\to}\frac{dJ_{\to}^{dis}}{dt}, \qquad \text{where} \qquad L_{\to} = \frac{\mu_0}{2\pi b}\ln\left|\frac{R_0}{r_0}\right|\int_{r_0}^{R_0} r\ln|r|\,dr. \qquad (46)$$

Note that the integral in the last expression is negative, so in the law "-" sign is not explicit. Thus, Lenz rule applies in the case of irrotational electromagnetic induction too. The essence of the phenomenon of irrotational electromagnetic induction is that, due to the induced charge displacement, it is created an EMF that opposes the radial displacement current. Thus, it is a reactance, which depends on the capacitive properties of the spiral coil. Formally, however, it should be attributed an impedance of the inductive type, since the phase voltage is $\pi/2$ ahead of current bias.

Equations (42) and (46) show that the inductive properties of a helical coil are characterized by two different factors: $L_\rightarrow$ and L_O. Obviously, there are two types of inductive reactances:

$$\text{circular} \quad X_{L(O)} = \omega L_O \quad \text{and radial} \quad X_{L(\rightarrow)} = \omega L_\rightarrow \tag{47}$$

Let us establish the phase relations between the vortex and the irrotational processes. The components of the current flowing in the primary coil have the same phase, for example:

$$j_O = j_O^{(0)} \sin \omega t, \quad j_\rightarrow = j_\rightarrow^{(0)} \sin \omega t.$$

The irrotational electric field induced in the secondary coil is determined by the differential equation (16), which should be written as:

$$\Delta \mathbf{E}_\rightarrow - \mu\varepsilon \frac{\partial^2 \mathbf{E}_\rightarrow}{\partial t^2} = \mu \frac{\partial \mathbf{j}_\rightarrow}{\partial t}.$$

Due to time differentiation, the phase of the vector $\mathbf{E}_\rightarrow$ (and, hence, $\mathbf{D}_\rightarrow$) is $\pi/2$ shifted with respect to $\mathbf{j}_\rightarrow$:

$$D_\rightarrow = D_\rightarrow^{(0)} \cos \omega t.$$

Consequently, irrotational displacement current varies with time according to the law:

$$\frac{\partial D_\rightarrow}{\partial t} = -D_\rightarrow^{(0)} \omega \sin \omega t,$$

that is –due to further time differentiation- it is in antiphase with respect to the original current flowing in the primary coil.

The equations (47) above express the *magnitude* of the inductive impedances , and has been written neglecting to their phases. Reactances in the tangential and radial directions should now be written taking into account the phase relations in the vortex and the irrotational processes, and the capacitive reactance of the ball antenna:

$$X_O = \omega L_O - \frac{1}{\omega C}, \qquad X_\rightarrow = -\omega L_\rightarrow + \frac{1}{\omega C} \tag{48}$$

The currents and voltages are individually represented on the vector diagrams (Fig. 26*a* and 26*b*). We first draw (Fig. 25*b*) the $\mathbf{j}_O$ current in the secondary coil: we set this vector as reference, with zero phase. As a consequence (Fig. 25*a*) we draw $\frac{\partial \mathbf{D}_\rightarrow}{\partial t}$ current vector pointing towards left,

since it is in anti-phase, as explained above. As known, the voltage developed across an inductor is $+\pi/2$ in lag with respect to the current. Thus $U_{L(o)}$ and $U_{L(\rightarrow)}$ vectors are oriented as shown in Fig.26b and Fig.26a respectively. Also, the voltage U_C across the capacitor has always $-\pi/2$ lag on the phase of the relevant current. The resulting voltages are thus *opposite* in the two cases vortex (Fig.26a) and irrotational (Fig.26a). When one process prevails on the other one, e.g. in resonances, the relevant voltage vector is predominant. Otherwise, the two U_C vectors will merge, subtracting each other.
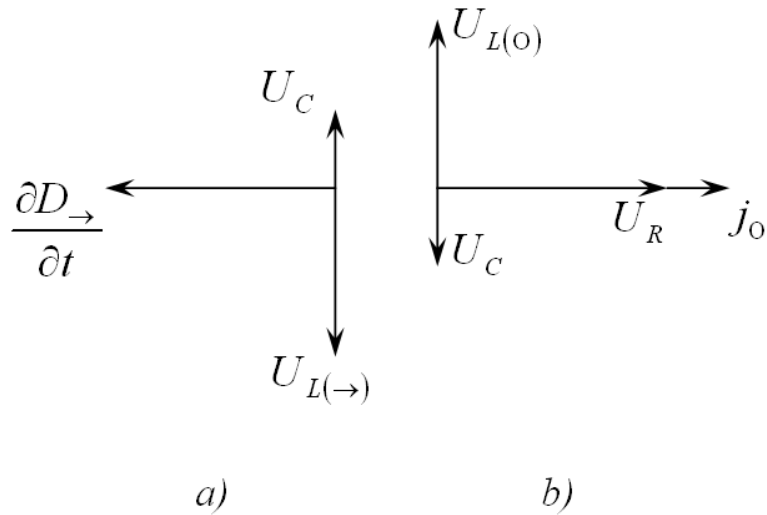

a)   b)

Fig. 26

We can figure out a simplified circuit as depicted in Fig.27.

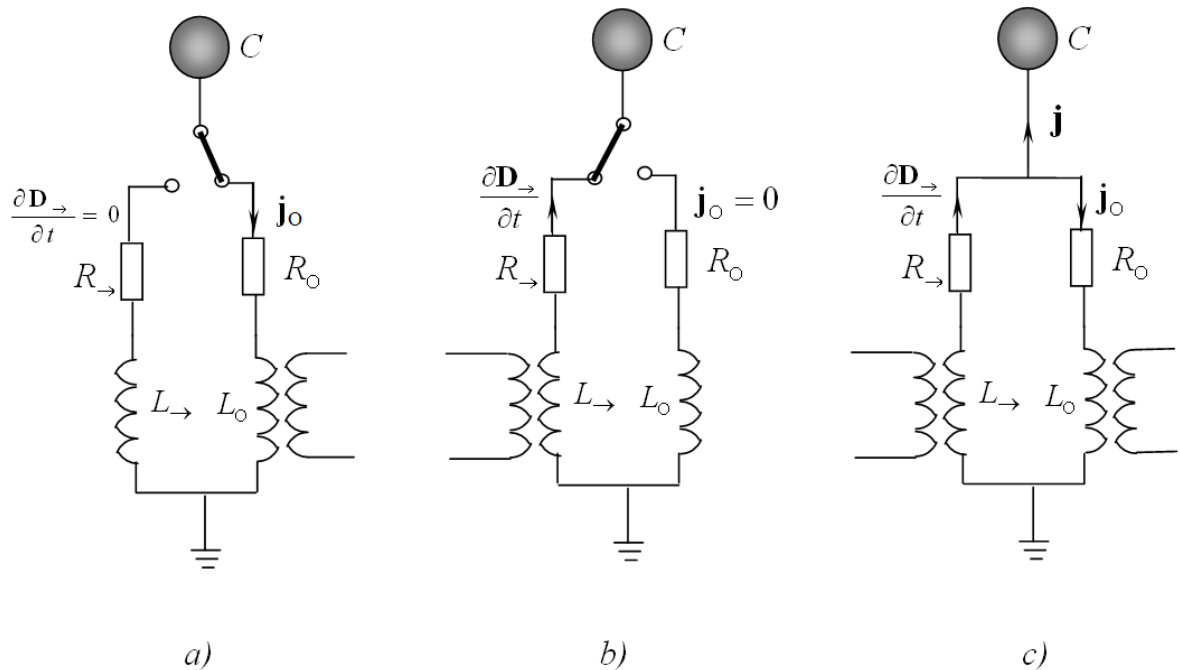a)   b)   c)

Fig.27

In this simplified model currents $\mathbf{j}_O$ and $\dfrac{\partial \mathbf{D}_{\rightarrow}}{\partial t}$ flow in two separate, parallel branches. When operating at a frequency f_{01} the current $\mathbf{j}_O$ goes on the right arm, because its reactance X_O decreases sharply $\left(\omega L_O = \dfrac{1}{\omega C}\right)$. The equivalent circuit is presented in Fig.27a. At a frequency f_{02} instead, the right arm is virtually opened, and reactance left branch $X_{\rightarrow}$ is minimal (Fig.27b).

The equivalent circuit when operating at a frequency of f_{03} is shown in Fig.27c. As the inductive elements with coefficients $L_{\rightarrow}$ and L_O are connected in parallel, the total inductance is given by the formula:

$$L = \frac{L_{\rightarrow} L_O}{L_{\rightarrow} + L_O}$$

In the wire connecting the spherical antenna the current is a superposition of $\mathbf{j}_O$ and $\dfrac{\partial \mathbf{D}_{\rightarrow}}{\partial t}$. Taking into account the phase relations of the resulting current is the Tesla coil is represented as a difference of eddy current conductivity and the radial displacement current:

$$j = j_O - \frac{\partial D_{\rightarrow}}{\partial t}.$$

In forming the third resonance peak at the estimated frequency of $f_{03} = 15 MHz$ a partial cancellation of the two opposite signals. On frequency response shown in Fig. 19 the all three peaks are visible. In other cases it may happen that the two signals cancel each other completely, and the third peak is not observed.

However, the circuit shown in Fig. 27, does not fully simulate the processes occurring in the coil of the Tesla. The first difference is that in this diagram in both branches flow currents of electrical conduction: we should not forget that one of them simulates the displacement current.

The second difference is that during the real experiment with the diagram shown in Fig. 27, the switch simulate two resonances separately. The merge of the parameters, giving the third resonance, cannot be modeled by it.

In the actual Tesla coil the three behaviours takes place automatically, depending on frequency. Therefore, the S_{11} frequency response shows the three peaks.

5.7 The role of Inductances in the resonance frequencies

In the laboratory test we have first explored frequency intervals in the HF (f<30MHz) range, due to the fact that the original Meyl experiment were in this

range. Here the resistive losses in the coils are more or less negligible, and the results of instrumental investigation are quite satisfactory. Also, some parts of the system can be considered lumped. Above 30MHz (VHF) the losses are very high, and stray parameters cannot be neglected. So the results are expected to have a fairly high degree of dispersion.

5.7.1 The range of HF

According the model mentioned in the previous section, it is possible to calculate three resonance frequencies. First, we study the resonance in the HF range:

$$\omega_{01} = 2\pi f_{01} = \sqrt{\frac{1}{L_O C}}, \quad \omega_{02} = 2\pi f_{02} = \sqrt{\frac{1}{L_\to C}}, \quad \omega_{03} = 2\pi f_{03} = \sqrt{\frac{1}{LC}}. \quad (49)$$

At frequency ω_{01} the azimuthal (circular) current $\mathbf{j}_O$ in a spiral coil increases. At frequency ω_{02} the picture changes significantly. There is a SMF, the gradient of which is directed along the radius of the coil. Due to this, the reactance in the radial direction is significantly reduced, so the radial current $\frac{\partial \mathbf{D}_\to}{\partial t}$ increases. This leads to the creation of a secondary coil in the centre of a strong alternating SMF, therefore, there arises an effective charge (potential) of large amplitude. We can say there is a "charge resonance".

At the third resonance frequency ω_{03} the *total* current $\mathbf{j}$ flowing in the spiral coil increases. In this case the minimum is the total reactance of the parallel branches of the circuit.

The conventional, azimuthal inductance L_0 can be calculated using the Harold Wheeler-approximation[4] [14]. This approximation is valid for the length of the wire winding up to half the length of the electromagnetic wave. In this case, the direction of the current in all areas of the antenna is changed simultaneously.

With the sizes and parameters used in our coils, the resulting inductance is $L_O^{(0)} = 44,7\mu H$. It corresponds to the frequency $f_{01} = 10MHz$. This value is in vicinity of the experimental value: $f_{01} = 9MHz$. The discrepancy can be explained by the presence of "stray" capacity, which can be estimated as 2-3 *pF*.

For vortical inductance the current propagates along the whole winding wire length, that, in out case, is about 6*m*. Consequently, only the operating frequencies lowest than $f = \dfrac{c}{2 \cdot WireLength} = 25MHz$ are compliant with the Wheeler approximation.

---

[4] An online calculator for flat spiral coil can be found at the following link:
www.circuits.dk/calculator_flat_spiral_coil_inductor.htm

However, for the approximate estimation apply the formula (46), which is determined by the irrotational inductive factor $L_\rightarrow^{(0)}$ approximation H. Wheeler. For a given size coils get:

$$L_\rightarrow^{(0)} = \frac{\mu_0}{2\pi b}\ln\left|\frac{R_o}{r_0}\right|\left|\int_{r_0}^{R_0} r\ln|r|dr\right| = -2.13\cdot10^{-6}\,\Gamma н\,.$$

Sign "-" corresponds to the Lenz law for irrotational electromagnetic induction (46).Estimated value of the corresponding resonance frequency:

$$f_{02} = \frac{1}{2\pi}\sqrt{\frac{1}{L_\rightarrow C}} = 45MHz\,.$$

The discrepancy between this and the experimental value $\left(f_{02} = 30MHz\right)$ is due not strict compliance with the conditions of H. Wheeler.

5.7.2 The range of VHF

Of greatest interest is the theoretical calculation of the basic resonance frequencies in VHF range, that is, beyond the approximation H. Wheeler.

We make the calculation of the basic resonance frequencies f_1, f_2 and f_3. To do that, we have to calculate the inductive factors. The length of the coil wire is about 6 *m*, and the length of the electromagnetic wave at the fundamental resonance frequency is close to 2 *m* Therefore, the length of the conductor corresponds to three traveling waves and creates a complex distribution of current density as a function of radius and polar angle $j_O(r,\varphi,t)$. The H. Wheeler approach in this case would not be satisfied. But an helical coil can be divided into several circular sections, each containing less than one half-wave. With this segmentation method each section complies with the Wheeler approximation.

We write the necessary formulas for a *n*-th section with an inner radius r_n and an outer radius R_n. Let us consider a generic circular alternating current with radius *r*. Such current, flowing through a conductor with a cross-section *ds* creates, in the center of the coil, a magnetic field (without delay):

$$dB = \frac{\mu j_O(t)}{2r}ds\,. \tag{50}$$

The area element of the radial cross-section of coil is:

$$ds = b\cdot dr\,.$$

As a result of the integration of (50) we get:

$$B_n(t) = \frac{\mu b j_{\mathrm{O}}(t)}{2} \ln\left|\frac{R_n}{r_n}\right| . \tag{51}$$

Substituting (51) into the differential equation (12) we get:

$$rot\mathbf{E}_n = -\frac{\mu b}{2} \ln\left|\frac{R_n}{r_n}\right| \cdot \frac{\partial \mathbf{j}_{\mathrm{O}}}{\partial t}$$

Now we multiply this equation by the surface area of the annular element coil: $ds_{\mathrm{O}} = 2\pi r dr$. As a result of the integration and application of Stokes theorem we have:

$$U_{\mathrm{O}n} = -\frac{\mu\pi}{2}(R_n + r_n)\ln\left|\frac{R_n}{r_n}\right| \cdot \frac{dJ_{\mathrm{O}n}}{dt} , \tag{52}$$

where $J_{\mathrm{O}n} = j_{\mathrm{O}}b(R_n - r_n)$ - the strength of a circular current of the n-th segment.

Comparing (52) with the law (42), we find the vortex induction factor for the n-th area:

$$L_{\mathrm{O}n} = \frac{\mu\pi}{2}(R_n + r_n)\ln\left|\frac{R_n}{r_n}\right| . \tag{53}$$

The table below shows a segmentation of the spiral coil used in our experiments; the results for each section and the total value of the inductive factor are calculated. To explore the inductance value around $150MHz$, as found in the VHF test (fig.12), the wave lengths involved are in the order of $2m$. The table below is the result for a segmentation with 6 sections.

Segment number	Inner radius r_n (mm)	Outer radius R_n (mm)	Number of turns	Number of turns inductive factor $L_{\mathrm{O}n}\left(10^{-6} H\right)$
1	5	25	12	0,094
2	25	35	6	0,039
3	35	42	4	0,027
4	42	48,5	4	0,024
5	48,5	53,5	3	0,019
6	53,5	58,5	2	0,018
Sum			31	0,222

The sections can be viewed as six virtual coils which are connected in series. The resulting inductance is defined by simple summation. Thus, as a result of calculations obtained value:

$$L_O = 0{,}222 \cdot 10^{-6} \, H \, .$$

The estimated value of the first group of VHF resonant frequency is in great agreement with the result of the experiment:

$$f_1 = \frac{1}{2\pi} \sqrt{\frac{1}{L_O C}} = 141 MHz \, .$$

Next, we perform a theoretical calculation irrotational inductive factor. in each of the selected segments using the formula (46):

$$L_{\to n} = \frac{\mu_0}{2\pi b} \ln \left| \frac{R_n}{r_n} \right| \int_{r_n}^{R_n} r \ln|r| dr \, .$$

Note, however, that the frequency of the second resonance peak $f_2 = 161{,}5 MHz$ is less than the half-wave length of 0.925 m and m in our case, the coil is 6.5 wavelength long, so, we divide the coil in 7 segments.

Each segment will represent the charge separation in the radial direction as well. In facts, in the radial direction each segment can be modeled as a capacitor. In presence of multiple segments, we obtain a system of series-connected capacitors. Let us depict a system of two series-connected capacitors of different values C_1 and C_2 (Fig. 28a). Adjacent segments are relevant to adjacent half-wave instantaneous charge distribution, thus having opposite sign.
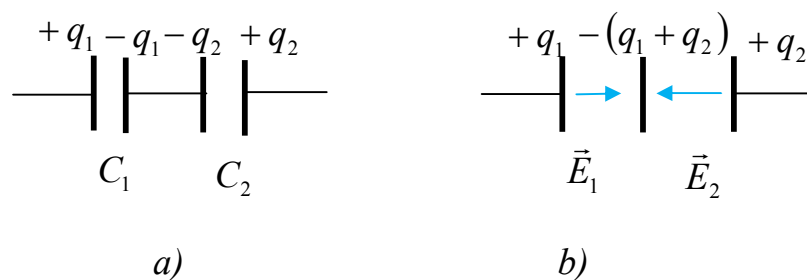

Fig. 28

This system can be represented as a non-homogeneous multi-layer capacitor (Fig 28b). Such a system can be replaced by a single capacitor, which creates a field:

$$E = E_1 - E_2 \, .$$

That is induced (irrotational) electric fields arising in adjacent segments are partially compensated. This is taken into account assigning alternating signs to the coefficients $L_{\rightarrow n}$ in the series computation.

Number	The inner radius r_n (mm)	Outer radius R_n (mm)	Number of turns	Section inductive factor $L_{\rightarrow n}\left(10^{-6}H\right)$
1	5	23	10,5	+0,262
2	23	32,25	5,5	-0,107
3	32,25	39	4,25	+0,023
4	39	45,5	3,5	-0,019
5	45,5	51	3	+0,015
6	50,5	55,5	2,75	-0,009
7 *(not complete)*	55,5	58,5	1,5	+0,004
Sum			31	0,169

Now, from the irrotational inductive factor value, we can calculate the frequency of the second resonance peak, almost identical to the test result:

$$f_2 = \frac{1}{2\pi}\sqrt{\frac{1}{L_O C_{\rightarrow}}} = 162 MHz .$$

Using the above values of inductive factors, we can get the resulting combined Tesla coil inductance:

$$L = \frac{L_{\rightarrow} L_O}{L_{\rightarrow} + L_O} = 0,096 \cdot 10^{-6} H .$$

This yields an estimated value of the third resonance peak:

$$f_3 = \frac{1}{2\pi}\sqrt{\frac{1}{LC}} = 215 MHz .$$

Such value is very different from the experimental $\left(f_3 = 179,8 MHz\right)$ one. A likely reason is that, at the frequency of the third resonance peak, f_3, the above choice of segmentation is not suitable to calculate the actual factors L_O and $L_{\rightarrow}$, since at the actual $\left(f_3 = 179,8 MHz\right)$ frequency, the half-wavelength value is 0.83m. Thus, we should adopt eight segments, instead. In the table below we calculated, $L_O(f_3)$ and $L_{\rightarrow}(f_3)$, with such segmentation, and, therefore, we are able to calculate the combined value $L(f_3)$.

Number	The inner radius r_n (mm)	Outer radius R_n (mm)	Number of turns	Section inductive factor $L_{On}\,(10^{-6}H)$	Section inductive factor $L_{\to n}\,(10^{-6}H)$
1	5	22	10	0,079	+0,238
2	22	30,5	5	0,034	-0,041
3	30,5	37,3	4	0,027	+0,024
4	37,3	42,8	3,25	0,022	-0,014
5	42,8	47,7	2,9	0,019	+0,011
6	47,7	52,15	2,6	0,017	-0,008
7	52,15	56,2	2,4	0,016	+0,007
8 *(not complete)*	56,2	58,5	0,85	0,009	-0,002
Sum			31	0,223	0,215

$$L = \frac{L_\to L_O}{L_\to + L_O} = 0{,}109 \cdot 10^{-6} H \qquad f_3 = \frac{1}{2\pi}\sqrt{\frac{1}{LC}} = 202 MHz \,.$$

This is a more accurate result, it differs from the experimental value by about 10%.

As it is clear, the obtained value, f_3, resulted from a segmentation choice that was to be set according to the f_3 wavelength itself, that usually is not known a priori. So, some degree of iteration could be needed in seeking a result.

6. Analysis of the new observed phenomena

6.1 Interpretation of the Faraday Cage phenomena

The experiments carried out using the Faraday cage led, as mentioned in the relevant section above, quite puzzling results. The cage shielding capability changes dramatically depending on the ground return wire connection to the cage itself.

Using typical criteria, it would be expected that no electromagnetic signal can be transmitted through the cage, when a small hole is present in the cage wall, if the size of such hole is *small compared with the operating wavelength*. In our experiment the operating wavelength (at the resonance) is about $30m$, and the hole diameter is about $0.01m$. In spite of this, in the first test configuration (Fig. 18) the transmission trough the Faraday cage could take place without any extra attenuation[5].

---

[5] At the resonances, the transmission loss S_{21}, has basically the same values as in the experiment on the table, without Faraday cage.

A possible hypothesis for this phenomenon is that a surface wave is transmitted over the "ground" wire itself. This kind of wave is a transverse-magnetic (TM) mode, thus longitudinal electric, and can be guided by and along the wire itself. However, we are not convinced by this hypothesis, since the transit of the wire through a tight hole in the cage metal wall should introduce a mode mismatch and impedance mismatch as well. In facts, the structure describing an insulated wire passing in the hole is basically a short coaxial line. As a matter of facts, the hole used was in facts a female N-N, 50 *Ohm*, pass-through connector, available in the Faraday cage patch panel. Only the inner conductor was used. The main mode in the coax section is obviously the TEM. Moreover, the estimated single-wire TM mode impedance is about 400 *Ohm* [18], so a fairly high impedance mismatch would be expected. This is not consistent with the (almost) zero extra loss obtained in the transmission parameter S_{21}.
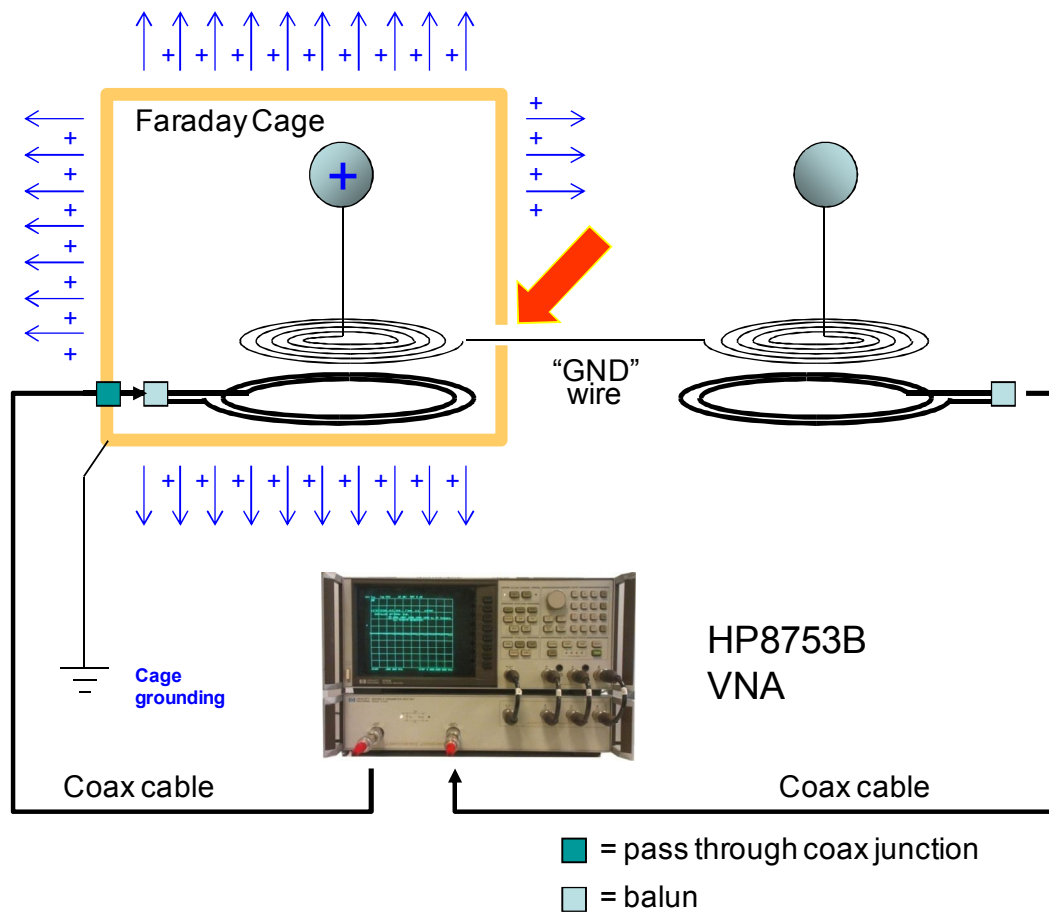

Fig. 29

The next hypothesis is based on the generalized electrodynamics. Let us consider the "Test 1" experiment, as depicted in Fig. 29. Due to the additional term $\varepsilon'\varepsilon_0 \dfrac{\partial B^*}{\partial t}$ present in the generalized equation (10), unsteady charge is created on the transmitting antenna. Also, the non-stationary SMF induced on

the metal surface of the cage becomes a variable electric charge. *The charges on the radiating antenna and the Faraday cage change in phase*. Thus, the cage itself become a transmitting antenna. Incidentally, the cage is grounded to earth through wires that have not negligible length (nor negligible inductance), so this doesn't prevent unsteady potential. In Fig.29 is shown the system at a time instant when the radiating antenna is positively charged. Faraday cage at this time, too, has a positive charge. Time-dependent electric field is created at the same time outside the cell. Thus, electroscalar waves are not shielded Faraday cage under the conditions of Test 1. This is a peculiar difference from transverse electromagnetic waves.

In Test 2 the sphere antenna and the Faraday cage formed a structure quite similar to a spherical capacitor: their charges at any time have different signs (Fig. 30). Electromagnetic process occurring inside the capacitor, does not go beyond it. Under these conditions, the Faraday cage effectively screened the electroscalar waves.
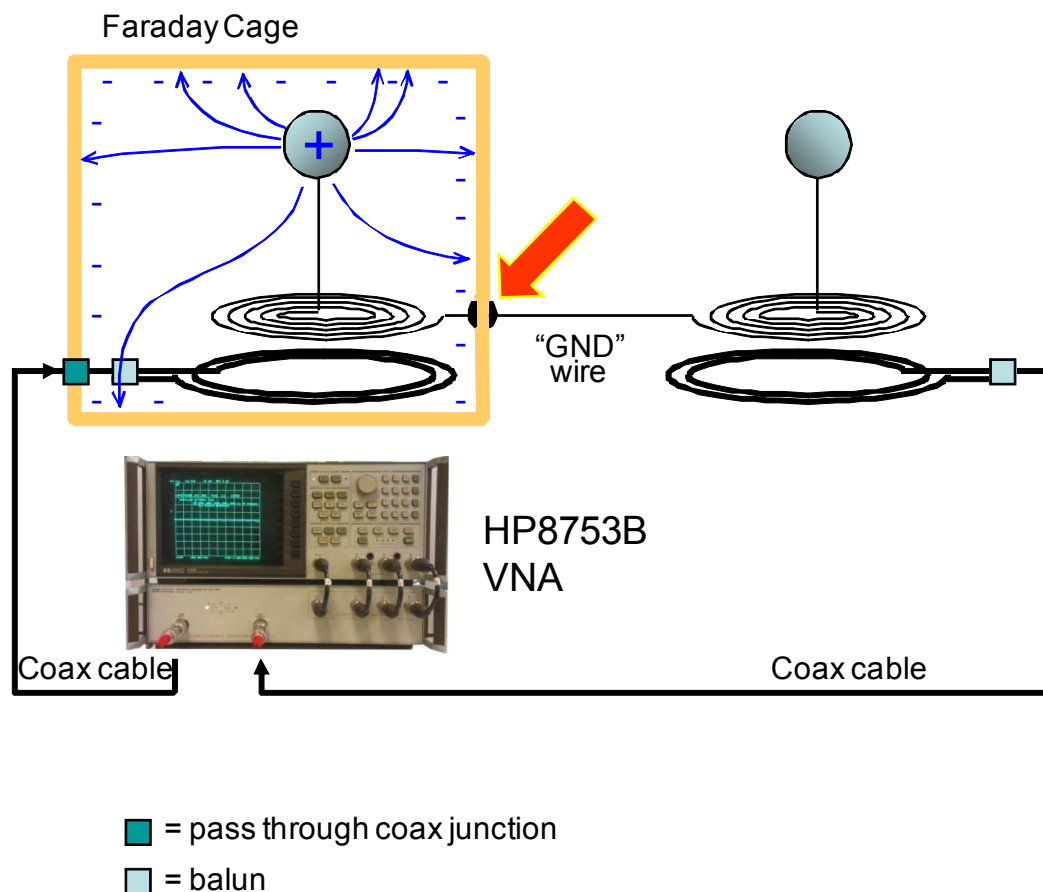

Fig. 30

7 Conclusions

In conclusion, we can say that the miniature experimental model of Meyl, cannot reproduce the whole experimental conditions of the original Tesla experiment. Obviously, those processes that take place at high voltage (high frequency), including those involving high slew-rates, cannot be reproduced.

However, the simplified, down-scaled Meyl set-up revealed some interesting and unusual aspects.

Most of the phenomena reported by K. Meyl have been observed and confirmed by us. The only exception is the claim of superluminal propagation velocity of electroscalar waves. This hypothesis has not found theoretical nor experimental confirmation.

We performed many additional experiments that revealed interesting new facts, namely:

• the independence of attenuation of the distance between the transmitter and the receiver (at least at the main resonance in the experiment). This could open interesting perspectives for communication and power transmission;

• the conditions under which a Faraday cage does not screen the electromagnetic waves emitted by a spherical antenna.

The hypothesis that the signal is transmitted from the Faraday cage with the help of transverse electromagnetic waves (TM), which spread along the ground wire is not considered satisfactory, due to the lack of any observed TM mode impedance mismatch loss, trough the Faraday cage.

The electroscalar waves model is a good theoretical tool with which explains the observed phenomena. A theory based on the generalized electrodynamics equations, adequately explains the mechanism of propagation of electromagnetic radiation and scalar waves. The processes occurring in the Tesla transformer, is well explained on the basis of representations of the vortex and potential electromagnetic processes. In particular, it is worth to be emphasized the role of the scalar magnetic field in the Tesla helical coils.

This research resulted in the following results:

• it is suggested that the signal propagation between the transmitter and receiver is carried by a electromagnetic wave process occurring between the spherical antennas;

• it has been shown that in this system the electromagnetic waves differ in their properties on the transverse Hertzian waves;

• The experimental results have been explained on the basis of the generalized (four) electromagnetic theory, which unites the vortex and potential electromagnetic processes;

• it is suggested that the signal transmission between the spherical antenna is performed by means of electroscalar waves;

• it has been established experimentally that the signal is transmitted without extra loss over long distances, which excludes the hypothesis of the capacitive coupling between the antennas;

• it has been theoretically described the operation principle of the Tesla transformer, consisting of two helical coils;

• it has been explained the cause of resonance with the three peaks;

• it has been theoretically calculated the frequencies of the resonance peaks in the HF-VHF range, in good agreement with the experimental values;

• finally, it has been investigated and described the mechanism of interaction of electroscalar waves with Faraday cage: in which operating

condition it performs as a shield, and, on the contrary, in which operating condition it is transparent to the electroscalar waves.

Bibliography

1. N. Tesla. Apparatus for transmission of electrical Energy. US Patent 649'621, 1900.
2. K. Meyl, "Scalar Waves: Theory and Experiments ", Journal of Scientific Exploration. Vol. 15, № 2, pp. 199–205, 2001.
3. H. Weidner, E. Zentgraf, T. Senkel, T. Junker, P. Winkels. Experiments to proof the evidence of scalar waves Tests with a Tesla reproduction by Prof. Konstantin Meyl. September 2001. http://www.gravitation.org
4. C. Monstein, J. P. Wesley, "Observation of scalar longitudinal electrodynamic waves", Europhys. Lett., 59 (4), pp. 514–520, Aug. 2002.
5. Николаев Г.В. Современная электродинамика и причины её парадоксальности. / Г.В. Николаев. - Томск: Твердыня, 2003.- 149 с.
6. Хворостенко Н.П. Продольные электромагнитные волны// Изв. ВУЗов. Физика. – 1992.- № 3.- С. 24-29.
7. Томилин А.К. Обобщенная электродинамика. – Усть-Каменогорск: ВКГТУ, 2009.- 168 с. http://vev50.narod.ru/Tomilin_ED.pdf
8. Tomilin A.K. "The Fundamentals of Generalized Electrodynamics", Physics e-print, July 2008. http://arxiv.org/pdf/0807.2172
9. Tomilin A.K. The Potential-Vortex Theory of the Electromagnetic Field. Physics e-print. Aug. 2010. http://arxiv.org/pdf/1008.3994
10. K.J. van Vlaenderen, A.Waser, "Generalization of classical electrodynamics to admit a scalar field and longitudinal waves", Hadronic Journal 24, 609-628 (2001).
11. Woodside D.A. Three-vector and scalar field identities and uniqueness theorems in Euclidean and Minkowski spaces// Am. J. Phys.,Vol.77, № 5, pp.438- 446, May 2009. woo09ajp.pdf
12. Борисенко А.И., Тарапов И.Е. Векторный анализ и начала тензорного исчисления. - Изд. 3-е. - М.: ВШ. 1966.
13. Purcell E. Electricity and Magnetism. Vol. II, 1965. 459 p.
14. Wheeler H. A. Fundamental limitations of small antennas.– Proceedings of the IRE, Dec. 1947, pp. 1479–1488.
15. Arbab I. Arbab, Zeinab A. Satti. On the Generalized Maxwell Equations and Their Prediction of Electroscalar Wave// Progress in physics, 2009, v.2.- s. 8-13.
16. Bruhn G. W. On Koen van Vlaenderen's Seventh Field Component Again. http://www.mathematik.tu-darmstadt.de/~bruhn/vV191005.html
17. Bettini G. Can electromagnetic scalar waves be radiated by a metal sphere? http://vixra.org/pdf/1109.0034v1.pdf
18. Elmore G. Introduction to propagating wave on a single conductor. www.corridor.biz/FullArticle.pdf